Feasibility assessment, process design and dynamic simulation for cogeneration of heat and power by steam reforming of diluted bioethanol

Antonio Tripodi[a], Elnaz Bahadori[a], Gianguido Ramis[b], Ilenia Rossetti[a,*]

(a) Chemical Plants and Industrial Chemistry Group, Dip. di Chimica, Università degli Studi di Milano, CNR-ISTM and INSTM-Milano Università unit, Via C. Golgi 19, Milano, Italy

(b) Dip. di Ingegneria Civile, Chimica e Ambientale, Università degli Studi di Genova, P.le J.F. Kennedy 1, I-16129, Genova, Italy and INSTM Unit Genova

Abstract

A bioethanol reforming system, capable of converting a diluted water-ethanol mixture into hydrogen, is sized and set up to produce 5 kW of electric power via a polymer electrolyte membrane fuel cells (PEMFC). A part of the produced hydrogen supplies heat for the reforming reaction without impairing the power generation, then no additional fuel is required. According to the different configurations of the control variables, the heat released from the system is distributed between two different temperature ranges and coupled to a standard house-scale combined heat and power (CHP) cogeneration apparatus. Hot water can be produced continuously at a high enough temperature to cover the need of a F-class home in the moderately cold Northern Italy winter climate. With a micro-accumulation solution and a careful choice of the set-points, also the sanitary hot water demand (DHW) of a 4-members family might be fulfilled with 2-3 daily cycles of the same system.

Keywords: Bioethanol Steam reforming; Fuel cell; Heat and power cogeneration; Feasibility; Dynamic simulation; Hydrogen production.

* Corresponding author: fax +39-02-50314300; email ilenia.rossetti@unimi.it

1 - Introduction

The production of electric energy for small-scale applications, using hydrogen as energy vector, relies nowadays on the already established fuel cell technology [1,2] coupled with efficient reforming catalysts and processes [3–6], that set renewable energy sources as viable alternatives to the traditional energy production and distribution chain [7–11]. Bioethanol, among other fed stocks, is very promising to meet the demand of the large market of distributed energy cogeneration [12,13].

With respect to reforming plants based on pure ethanol [14,15], different strategies make use of less expensive diluted bioethanol [8,16–18], while a recent technology as the directly-fed fuel cells has the drawback of missing a dedicated CO purification section [19].

In this case, the system is much more flexible both for the fuel supply and for the possible operation modes, provided that the additional heat input required to vaporize excess water quantities can eventually be retrieved as useful thermal energy.

The small-scale power production based on bioethanol is even more promising if it meets also the distributed market of co-generation, which is crucial to increase the overall energy saving and renewable source utilization in developed countries [20,21]: in fact, house-level cogeneration is useful to exploit the solar radiation [22,23] or to increase the value of traditional sources such as methane [24,25] or natural gas [21,26] and gasoline [20] (respectively the main feed stocks of the distributed or autonomous consumption), beside hydrogen itself [27]. Comparative technologies for sustainable hydrogen production are currently under study. However, they are best fitted to large scale applications. For instance, net plant efficiency of 46.4% compared to those of the GE Energy and Shell Convective plants (39.2% and 42.0%, respectively), were reported by Esmaili et al. [28].

A techno-economic analysis on the steam methane reforming (SMR) for low-CO_2 hydrogen production was carried out by comparing alternative routes: (i) Electrolysis from renewables; (ii) Reforming of hydrocarbons with carbon capture and sequestration (CCS) and (iii) Pyrolysis [29].

Two technologies for chemical looping combustion (CLC) with CO_2-capture were applied to a coal-based IGCC (Integrated Gasification Combined Cycle) power plant [30]. In the same frame, a comprehensive exergoeconomic evaluation and comparison of combined-cycle power plant generation has been set, obtaining higher exergetic efficiency of 58.3% for the H-Class, while this value is calculated to be 56% for the F-Class turbines [31]. Sorption enhanced reforming with in-situ CO_2 capture has been also investigated on a large scale (200 kWth pilot plant) [32]. A micro-combined 10 kW heat and power generation system based on fuel cell has been also analysed from the exergoeconomic point of view [33]. Small, residential size systems have nowadays a higher expectation to be exploited because of the limited investment needed. Thus, it is particularly important to focus on feasibility assessment, detailed design and optimisation of small scale systems.

With this work, we propose the detailed design of a residential size cogeneration system based on a bioethanol-to-hydrogen-to-power technology. The basic layout and preliminary sizing of a water circuit has been also performed, that recovers a substantial fraction of the waste heat released by a bioethanol reforming unit already sized to meet a home-scale power production of 5 $kW_{electric}$. This turns the system into a full Combined Heat and Power (CHP) plant (see also [34] and [22] for a review of FC-based CHP). The thermal energy is sufficient to cover the steady-state wintertime dispersion for a class ‘F’ two-storey house in the Northern Italy climate with a traditional radiation system [35], while the more demanding sanitary hot water (DHW) production can be met by resorting to a micro-accumulation strategy. The flexibility provided by a diluted hydro-alcoholic feed mixture with a separate reformer-fuel cell layout makes it possible to tune the system performance according to the instant house need, and the use of hydrogen as a *vector* rather than as a source let foresee an easier feedstock supply and management.

2 – Methods and models

The calculation of the reforming apparatus has been performed using Aspen Plus® V8.8 with the PURE32 Databank. The Peng-Robinson and Non-Random-Two-Liquids (NRTL) thermodynamic systems have been employed for the whole flowsheet, while for the simpler steady-state radiators power we adopted the STEAM-TAB plus PENG-ROB packages. These thermodynamic packages were compared for predictions with rival models against experimental data and demonstrated appropriate. The dynamic simulation of the hot water delivery has been modeled and solved with Matlab® V7.10 (using the 'ode45' algorithm to integrate the differential equations). The algorithm used to estimate a model house heat dispersions according to best professional practices (*vide infra*) runs on MS Excel™. This was done to ensure better adherence to the designed unit with respect to models embedded in the Aspen Dynamics package.

2.1 - Ethanol reforming system layout

The ethanol reforming system is based on the one already proposed in recent papers [16–18]. Basically, the cogeneration plant is constituted by an ethanol steam reformer, which is thermally sustained by a burner. The latter uses part of the reformate as fuel. The reformate is fed to a fuel cell which needs very straightforward purification from CO (< 20 ppmv), which is accomplished by a series of High- and Low-Temperature Water Gas Shift (HT-WGS and LT-WGS) and a methanator. Ethanol with different water content is fed to the system, aiming at exploiting diluted bioethanol solutions, that allow considerable cost saving with respect to azeotropic ethanol [16,36–38].

The main features are as follows, with reference to Figure 1 for a simplified system diagram:

a) the hydro-alcoholic feed mixture is pre-heated in the feed-to-product exchanger 'FPHX' by the hot reformate, then it is vaporized and overheated in the 'AUTOHX' exchanger before entering the steam reformer 'SR' at the set temperature of 567 °C;

b) the hot utility to vaporize the feed and supply the reaction heat is the hot gas outflowing from a burner, which oxidizes the residual methane deriving from the various reactors and part of the produced hydrogen;

c) the reformate undergoes further CO conversion into CO_2 and CH_4 in the two WGS and methanation stages, then is cooled in the condenser to discharge excess water, and is finally fed to a polymer electrolyte membrane fuel cell (PEMFC), which operates at 80 °C;

d) the exhaust flue gases exiting from the reformer jacket and from the AUTOHX are further cooled down in the 'FlueHX' before being discharged.

The other specifications of the blocks are essentially as follows:

a) the reformer is a 'Plug Flow Reactor' block with 100 tubes (1 m long, 7 mm wide) containing 18 grams of catalyst (deposed as coating) and heated in equicurrent flow arrangement, the reaction stoichiometry is reported in Table 1 and is extensively described elsewhere [39];

b) the heat exchangers are shortcut 'HX' blocks specified with fixed outlet temperatures, save for the crucial AUTOHX block, which is modeled as a rigorous two-side exchanger (LMTD method with nested Broyden convergence) with an overall UA = 50 W/m^2 °C x 2 m^2 = 100 W/°C. This choice was made because the PFHX block deals with cold/hot fluids having roughly the same heat capacity and the same mass flows under different condition, while the other block experiences more variable operating conditions that need to be addressed with a realistic adjustment of the controllable variables;

c) the water-gas shift and methanation reactors are modeled as 'Equilibrium' reactor blocks, which workout the two stoichiometries:

$$CO + H_2O = CO_2 + H_2 \quad \text{(R1)}$$

$$CO + 3H_2 = CH_4 + H_2O \quad \text{(R2)}$$

as described in [18] – see references therein also for the choice of the fluid inlet temperatures equal to 350 and 210 °C, respectively. Notice that the Aspen PLUS® flowsheet

actually employed foresee additional intercoolers and refrigeration duties for these blocks, but they have not been represented since the thermal power of this stages is lower than 5% of the total;

d) the condenser is modeled as a 'Flash2' block, its working temperature (50 °C) has been chosen to keep the water vapor concentration in the gas within the limit of 10% with respect to the hydrogen flow;

e) the burner is modeled as a 'Gibbs' reactor that yields the thermodynamically more stable mixture derived from the H_2 spared from the fuel cell (together with the produced methane and other residual byproducts) in presence of an over-stoichiometric oxygen quantity, then simulating complete oxidation.

2.2 - Reforming system working specifications

The main function of the above described system is the electrical power production. Ethanol flowrate of 70 mol/h has been selected in order to provide 5 $kW_{electrical}$, assuming that the FC has an electrical efficiency of 40% [20,21] and knowing the molar hydrogen yield from previous experimental, kinetic and simulation studies [16,17].

The cell power output depends essentially on three system variables:

a) the fuel cell reformate utilization factor (*x*). This fraction derives from the intrinsic capability of the FC used, but it can also be regulated by a reformate split upstream the cell: since in this model the cell is a 'STOICHIOMETRIC' type reactor which brings the oxidation:

$$H_2 + \frac{1}{2}O_2 = H_2O \qquad \text{(R3)}$$

to the specified level of hydrogen molar conversion, *x* actually describes both items and the values tested here were 0.5 – 0.6 – 0.7 – 0.8 – 0.9;

b) the amount of burnt gases flown through the steam reformer jacket determines the heat available to sustain the reforming and, consequently, the hydrogen yield. The hot utility temperature depends on the fuel burnt (and from its dilution with the oxidant air), and then it is not considered as an independent variable. It is set through the opening of a valve and the tested range for the valve 'FlueS1' was 0.25 – 0.55;

c) the water content in the feed determines the heat subtracted from the burner gas to vaporize the feed. The higher the ethanol dilution in the feed, the higher the heat needed to vaporize it, but the lowest the duty spent for ethanol purification and dehydration upstream. However, such heat is released as condenser duty, shifting the total thermal output from the hot utility to a lower temperature heat source. From a chemical point of view, a high water concentration is preferred, since it enhances the CO – CO_2 shift and the coke reforming. The values here tested were 5 – 7 – 9 moles of H_2O per mole of ethanol, set through the valve 'CondS'. Higher water amount allow also the exploitation of more diluted (less expensive) bioethanol solutions.

To bring the fixed process condition to their target values according to these variable inputs, the following automated 'interlocks' were implemented, by using Fortran 'Calculator' blocks or 'Design Specifications', with the 'Secant' convergence algorithm (see also Figure 2):

a) the heat exchanger AUTOHX between the feed and the hot gases is *oversized*, so that the FeedS valve opens and closes in order to keep the fluid temperature at the reformer inlet fixed at 567 °C: downstream this block is placed another HX block (not shown) that acts as a 'safeguard' to allow the reformer simulation be carried out also whether the above specification should not be met. The duty of this block was nil (within the tolerances) in all the cases reported in this work. It should be stressed that this additional HX also provides an additional degree of freedom to guarantee stable operation and will be useful in further dynamic simulation;

b) the FlueS2 valve opening set point depends on the feed dilution, on the fraction of flue gases that bypasses the reformer and on their overall enthalpy content as determined by the FC efficiency. A wrong specification of this block determines an improper calculation of the AUTOHX, which in turn results in various parameters going out of range according to time-to-time simulation details. To avoid excessive computational effort and convergence problems (also because the specification target is not so easily defined), the valve opening set point has been first tested manually in every case. On this basis, Tables 2 and 3 list the FlueS1 set points allowed for each *x* and CondS values. Accordingly, for every feed dilution level, the FlueS1 optimal value was extrapolated as a parabolic function of *x* implemented in a dedicated 'Calculator' block;

c) the air flow to the burner and the cell is calculated automatically from the hydrogen (and methane) flow at the inlet of these two blocks, to grant 110% of the stoichiometric oxygen.

2.3 - Cogeneration system layout and calculation

As the ethanol fed to reformer amounts to 70 mol/h, it provides roughly 26.7 kW (calculated from its standard-state oxidation enthalpy [40]). Thus, besides the output electrical power, the global system efficiency is significantly increased by a cogeneration system capable of exploiting the heat released from: i) the Condenser (at 50 °C), ii) the FC (at 80 °C) and iii) the FlueHX block (cascade from a variable temperature always above 300 °C down to 80 °C, since a forced flow system does not require hotter gases), being these the only 3 points for usable energy output.

The reforming system has to be constantly online to produce continuously electric power (to be used in house or sold to the grid), so the cooling of the above mentioned blocks is needed to ensure plant operation. Therefore, the cogeneration system (Figures 3 and 4) is thermally connected with a water Reservoir ('R') that stores the available enthalpy over time [26,34] and an air-cooled exchanger that discharges indirectly the power still in excess with respect to the present house needs and reservoir dispersion. The integration of a DHW supply follows the strategy of the network

water micro-accumulation (at the same temperature of the reservoir) and on-demand further heating, rather than resorting to more complex stratified accumulation strategies [24].

The limiting design feature of the cogeneration system is the low reservoir temperature (40 °C) needed to assure the cooling of the reformate condenser, which implies that any other appliance (*i.e.* the house radiators or the sanitary water production) has to be fed on-demand with the higher-temperature heat of the PEM-FC and the flue gases. Always for this reason, the sanitary circuit bulk volume is supposed to be contained within the larger reservoir tank in order to take advantage of a heat contact extended over time.

At this stage, the layout has been kept as simple as possible supposing that the same water used for the reforming system cooling can be used directly for the radiators: the valve 'R1' splits the recirculation flow after the condenser and the FC-Flues HX (Heat Exchanger) pair, because the flowrate needed to keep the cold-side of the condenser HX within 4-5 °C from the hot side (such a low delta T is feasible due to the high heat exchange coefficients of condensing fluids) would prevent water from reaching the temperature range of 65 – 75 °C needed for a radiator circuit [41–43]. The water returning from the radiators, from their bypass line and the condenser is collected before an air cooler that dissipates the heat not yet dispersed from the house or the reservoir. The sanitary water heating, whose activation disables the radiators network and the air cooler, is placed in parallel via the commuter 'D'.

The calculation of the steady state cooling of the reforming system has been done placing virtual heat exchangers 'HX' blocks that transfer to the service water the heat coming from the various blocks: at this stage of development, the exchanger surfaces have not been assessed yet. The heat and water flows of the radiators has been calculated as follows:

a) the power calculation follows the recommendation and the cross-checked reference values of different vendors and models [43,44], based on the formulation:

$$q = q_{ref}\left(\frac{T}{T_{ref}}\right)^{n}$$ [41],

where the external air temperature has the reference value of 20 °C [26] and q_{ref} is given for a fixed water-air temperature difference;

b) the radiators water inlet and outlet temperatures have been evaluated as 70±5 and 43±3 °C [41–43];

c) this temperature range has been divided into 10 intervals, and for each the formula defined in *a)* has been applied. The heat is then the sum of this step-wise calculation and has to be consistent with the lump calculation supposing a mean water temperature of 55 °C and a mean water-air ΔT =33 °C;

d) the radiator surface has been estimated to be circa 0.65 m^2 for the size and plate numbers as reported in the above cited references, this allows to assess the specific heat exchange coefficient (U) from the gross exchange coefficient (UA);

e) the specific heat exchange coefficient has then been compared with the theoretical calculation using the correlation:

$$Nu = 0.13 \times (Gr \times Pr)^{0.33}$$

for Gr >10^9 over a vertical plate [45] (Table 4). In the formula, Nu = Nusselt number, Gr = Grashof number and Pr = Prantl number.

f) the air flow has been calculated *a posteriori* to match the calculated radiator duty with a supposed temperature increase from 15 to 30-33 °C. At this stage this issue has not been investigated further, since the real values of these parameters are deeply affected in a complex way by the relative position of each radiator in every room and by the room shapes and wall exposition, which determine the natural convection cells behavior.

A total number of 91 radiator elements (and then the service water flow after the reformate condenser) has been calculated to cope with a dispersed heat of 9 kW, corresponding to the need of a class ‘F’ flat in Northern Italy in winter (climate code: E2404). This calculation has been done according to the DOCET V3.5 algorithm [35] (this package cannot calculate the energetic performance of complex cogeneration systems, but is compliant with the Italian Law: DM

26/06/2015 “National guidelines for the energetic performance assessment of buildings”, Annex I, for what concerns the heat dispersion of a building) and is reported in Table 5 (other literature calculations based on recognized datasets for building materials and climate lead to very similar results [26]). The radiators have then been modeled in Aspen PLUS® as rigorous two-side heat exchanger ‘HX’ blocks.

The sanitary water production follows a different strategy, due to the fact that even a target consumption level of 10 L/min [26,46] and relatively low temperature set point of 45 °C [26,47,48] (though even lower set points may be considered for energy saving [49–51]) cannot be met during winter (grid water was assumed at T = 5 °C as conservative case) with the available reformate thermal power (*ca.*18 kW). On the other hand, relatively low accumulation volumes of 150 – 250 L are the normal supply for a 4 members family (see [47] and references therein, and also [51] for typical commercial systems), so the calculation has been performed as follows in a *dynamic* framework using a specifically developed MATLAB® code:

a) the reservoir tank and the sanitary water accumulation volume are represented as fixed/variable masses of water, whose enthalpy content is related to their mean temperature (‘perfect mixing’ assumption [47]);
b) the heat exchangers are split into two parts with three relevant faces (inlet – mean point – outlet). For each of them, the exchanged power is calculated via the Number of Transfer Units (NTU) method for a single pass shell & tube heat exchanger;
c) the DHW simulation is performed at fixed water flows and the temperatures reached are the interesting state variables. So, the calculated duties are aligned to the values needed by each block (as retrieved from the Aspen PLUS® simulation of the reforming system) by varying the global heat exchange coefficient UA of the exchanger;
d) since the heat exchangers powers vary according to the temperature difference over time, the UA adjustment is achieved at each simulation step by a recursive routine for each exchanger

– this is equivalent to fix a UA value and varying the recirculation water flow, but is computationally simpler since each device can be treated on its own.

The equations governing the system and the nominal conditions are collected in Tables 6 and 7.

2.4 - Cogeneration system working

When there is no need for sanitary water, the reservoir total circulation is regulated so to keep the condenser HX cold side within 45±1 °C (see also [52] for the choice of the parameter), while the valve ‘R1’ split fraction is calculated in order to make the radiators inlet water as hot as 70±1 °C. The air cooler is then specified so to cool down the return water to the same starting temperature of 40 °C, then closing the reservoir tank heat balance. Any dispersion to the environment is implicitly addressed by the fact that a colder reserve would feed the condenser HX with less water maintaining the same temperatures at the other circuit points: the check condition for the feasibility of this operative mode (satisfied for all the presented cases) is the presence of a small hot water flow in the radiators bypass line.

When the DHW production is activated, the radiators line is closed, the air cooler stopped, and all the recirculation flow is routed either to the reservoir (to maintain the bulk of the enthalpy store) or to the sanitary HX ‘X’ (to achieve the desired over-heating [52]) through the splitter D. In this case, all the water flowing through the condenser HX (determined so to stay 4-5 °C below the hot side temperature during all the simulation time) passes through the FC and gas HXs, because even reaching final temperatures as low as 60 °C, there is still enough margin with respect to the sanitary water set-point.

The D valve opens over time to avoid an undesired hot water surge in the first instants followed by an inefficient utilization of the heat stored in the reservoir. If the hot water demand prolongs over a certain time (15 minutes in the case presented), then the network cold water supply into the sanitary circuit is discontinued until the water reservoir falls down to a selected threshold (150 of the initial 300 L), so stopping the sanitary water cooldown. The D split opening is tuned over time, within the

derivatives calculation routine, as reported in Table 6, while the cold water supply enters or not the system mass balance according to an on-off logic.

Since the steady state radiators calculation and the dynamic sanitary water supply are done with different software and represents two mutually excluding cases, there is no actual representation of this fundamental switch of the cogeneration system neither in the Aspen PLUS® flowsheet or in the MATLAB® scripts.

3 – Results and discussion

3.1 - Stability and operative ranges of the reforming system

A summary of the key specifications and results for the different blocks of the flowsheet are reported in Table 8. The main variable that determines the cell power output is the hot gases flow through the steam reformer, which causes a variation as large as the 25% of the reformer hydrogen production and then of the cell power output for the tested range (0.25 – 0.55) of the split fractions (an extensive discussion and details are reported in [18]). Also the heat released by the spent flue gases in their final cooling before venting is, as expected, deeply affected by this parameter, varying as much as the 50% of the largest value (that corresponds to the flue split fraction of 0.25).

The fuel cell utilization factor has its larger effect on the hot flues residual heat. Keeping fixed all the other conditions, as x varies from 0.5 to 0.9 then the power needed to cool the gases down to 80 °C drops to the 50% or even the 35% of its larger value (that is obtained for x = 0.5). While high x values affect negatively the hydrogen production (lower fuel to the burnermeans lower heat supply to the endothermal reaction), the gross cell power is scarcely modified, because the positive effect on the FC working compensates the phenomenon.

The water content in the feed has little effect on the cell power output, because within the tested range (5, 7 and 9 moles of water per 1 mole of ethanol) the alcohol is always the limiting reagent of the steam reforming reaction. On the other hand, the residual heat content of the flue gases varies dramatically as they have to vaporize increased water amounts in the AUTOHX block. Moreover,

larger water excess pushes forward the WGS equilibrium, leaving less CO to be converted into methane and then burned. Thus, also the combustion gases temperature decreases. The duty for the feed-to-product (FPHX) exchanger is nearly constant, because the heat capacity of the cold and hot sides varies in the same way, while the cooling duty for the reformate condenser increases sensitively.

3.2 - Power outputs distribution

The effect of the above described results are drawn in Figure 5 that represents the distribution of the total system power between the relevant outputs fixing the reformer heat input (40% of the hot gases flow admitted into its jacket) and controlling the cell utilization factor and the ethanol dilution. It is evident that the cell power is related essentially to the utilization factor itself, while the water recycled from the condenser to the feed shifts the proportion between the condenser duty and the hot gases residual enthalpy.

Fixing instead the cell *x* (*e.g.* to the value of 0.7), the whole range of hot flues split is explored in Figure 6 for the different water contents in the feed. The cell reacts positively to the enhanced hydrogen output and to methane decrease, while the condenser duty is very sensitive to the dilution level, but scarcely affected by the gas utilization (as expected, as the water latent heat represents most of this duty, regardless of the detailed reformate chemical composition).

On this basis, eight working modes have been selected to test the possibility of the cogeneration system to cope with different operations of the reformer (Table 9). Two modes (‘4’ and ‘5’) feature a low electric power output (3 $kW_{electrical}$ instead of the 5 rated) and represent ideally a night-time working mode (or when the house is left for a few days): they differ for the trade-off between the condenser duty and the flue gases heat. This is the difference also for the working modes ‘1’ and ‘2’, which, however, display a full electric output. The working points ‘3’ and ‘6’ show the highest condenser duties and are differentiated by the heat distribution between the cell and the flues. The cases ‘7’ and ‘8’ have been chosen to test the highest utilization factor. We have to point out that

the selection of two different electric loads does not represent a true “variable load” strategy (as in [53]), because the overall enthalpy input of the system is fixed by the ethanol flowrate.

A full points representation of the variable state-space has not been adopted because of the implicit correlation constituted by the fixed total power, which rules out one degree of freedom. Moreover, the flue gases duty is not a real state variable for the reforming system (while the flues split before the reactor is), but it represent the actually relevant parameter affecting the cogeneration system.

3.3 –Operating modes of the cogeneration system

The steady state calculation for the cogeneration system is reported in Tables 8-10, coupled with the selected working points of the reforming system. The maximum target house demand, 9 $kW_{thermal}$, is always met, with a reserve bypass flow of hot water still available and with a radiated power (for single radiating element) always within the range extrapolated from the data supplied by vendors [43,44] or from the literature [41] (see also Table 4). This result is achieved controlling only the total recirculation flow and the split fraction of the cold water exiting the condenser.

Any additional heat transfer from the reservoir circuit to the environment (or toward the sanitary circuit) is compensated, during this operating mode, with a lower temperature of the circulating water that makes the air cooler fan switch off, until the residual power left in the bypass line re-heats the reservoir.

For every case, the foreseen consumptions of the air fan are also reported, in the hypothesis that 1000 m^3/h of dry air have to overcome a pressure drop of 5 mbar. The limiting case, from this system point of view, is the summer period when the radiators are not used and the cooling air is hotter (assumed mean value 25 °C). A separated calculation for three representative working points is reported in Table 11: though the foreseen values of the heat exchange coefficients are high (roughly 100 m^2 of HX surface supposing the liminar coefficient *h* of the order of 10 W/m^2 °C), this system can be conveniently split into modules and installed independently.

The theoretical efficiency of the whole system is, averaging the tested case, as high as the 79.7%: this value is limited by the fact that the reforming system effluents cannot be reasonably cooled below 80 °C, otherwise the radiators water could not reach the 70 – 75 °C range that best fits this application [41]. Moreover, the final heating takes place in a liquid-gas exchanger, which has the lowest exchange coefficient, at fixed area. The actual energetic yield is lower (but always higher than 50%) because the thermal energy required in this study is relatively low (a class F flat) though in line with average European data [47]. In the case of hot summer days, the global efficiency is limited to the 18% relative to electrical production, only. The heat to power ratio of the steady-state cases ranges from 2 to 3, but comprises also the hydrogen yield of the reforming system and it is not directly comparable with values based on the FC alone [34,47].

3.4 - Sanitary water yield

The dynamic simulations for the DHW are reported in Figure 7. The first screening of the reforming system working states has been done imposing a fixed opening level of the D split (0.33 L/L) and a continuous feed of cold water from the network (the worst case of 5 °C water inlet temperature is considered). As expected, the best cases (ID ‘4’ and ‘5’, Table 9) are those with a limited electric power output (just 3 kW).

For the best case (ID ‘4’), the effect of the D valve dynamic tuning has been tested inputting two different initial opening (0.22 and 0.10) and then letting vary this parameter with an opening rate proportional to the difference ($T_{hot} - T_{setpoint}$) at constant gain. The gain value has been selected heuristically, since the overall transfer function for the whole system has not been derived and the time step of the equation solver varies dynamically. In any case, the numerical stability of the simulation was not affected by this parameter. The beneficial effect of this strategy (Figure 8) is evident in prolonging the hot water supply within ±1 °C from the set point for more than 15 minutes, while also damping the unnecessary hot surge occurring at the system startup.

To grant a hot water supply of 10 L/min for a longer time interval, however, it is necessary to exploit the sanitary circuit reserve without reintegration, as represented in Figures 9 and 10. As expected, once the cooldown due to the external supply stops, the hot temperature increase again and is maintained until the low level threshold is reached and the cold water enters the system again. This strategy prevents the water temperature to fall below 40 °C too early even in the worst tested case (ID '6'), and substantially enhances the system performance in the best case (ID '4'), leading to a 35 – 40 minutes availability of hot water within 1 °C from the setpoint with the D split still at partial opening. Within this 'depletion' strategy, it is also possible to reassess the feasibility of the third best case (ID '1'), which is characterized by a full cell electric output of 5 kW. Despite the initial cooldown somehow deeper than in the best case, and the eventual recover steeper (the valve D in this case re-opens completely), the performance is still in line with the low cell output scenario, opening the possibility of relying on the water storage feature to cope effectively also with cases of heavy household electrical consumption.

Moreover, reported data on the *average* DHW heat consumption are of the same order of magnitude of the electric need of the house [54], indicating that a refinement of the accumulation system is a realistic alternative to higher fuel inputs.

Notice also that the foreseen timescales of this subsystem are compatible with the response of a typical methane reformer under changing working conditions [55], due to thermal inertia of water.

3.5 - Temperature increase

From the reported analysis, it is clear that the bottleneck for the sanitary water production is the low temperature of the reformate condenser, which forces the cogeneration reservoir to be kept under the sanitary water set-point. For this reason, the possibility to raise the water separation (condenser) temperature of 5 °C (from 50 to 55 °C) has been evaluated.

a) Reformate production: as shown in the parity plot (Figure 11), the hydrogen absolute content at the reactor exit does not change and this means that the reforming conditions are maintained even with the slightly colder gases produced by the burner.

b) Reformate water content: as expected, the water *absolute* content at the FC inlet increases (maps 12), but the feed dilution has no effect on this phenomenon. This is due to the fact that liquid and gaseous water increase in the same way, downstream the reformer, while higher x values rises the mixture dew point (thus lowering the water content in the condenser vapors) because they determine a reformate poorer in hydrogen. This effect is visible also in the charts 13, whose *apparently* opposite trend of the *relative* H_2O/H_2 reformate content is correctly explained in this way.

c) Cogeneration balances. The reforming block duties are insensitive to this temperature shift (the condenser and the PEMFC dissipate a latent heat, and the flues temperature does not change much). The radiators balance takes advantage of the higher water temperature achievable, while the dispersed heat is nearly equal (also the set point of the air cooler is higher), so the global energetic yield rises, on the average, from 52 to 55%.

d) Sanitary water production: the sanitary water set point can be increased to 48 °C [49], in line with the commonly recommended target of 50 °C [11,48], achieving even better performances, over time, than in the other scenarios. In fact, if the best cases (‘4’ and ‘41’) grant the same overall time of water within ±1 °C from their respective set points, the more interesting case ‘11’ (featuring a full electrical yield) shows a tighter set point compliance, also due to a more careful control of the D split. In this context, also a case with the flue gas heat nearly equal to the condenser one (71, same Figure 10) can maintain a moderate set point of 46.5 °C for 40 minutes. Other studies [52,53] indicate that a higher reservoir set-point (and possibly a more refined accumulation layout) achieves superior DHW delivery performances even with less than 12 kW of available heat.

Table 12 summarises an overview of energetic performance. The results for the overall efficiencies are also in line with a detailed sensitivity analysis for an ethanol reforming system [56], run on Aspen Plus® as well.

4 – Conclusions

An increased water content in the feed, *i.e.* the use of diluted bioethanol, has an overall beneficial effect on a steam reforming system for hydrogen production. On one hand, the heat subtracted to the burned gas downstream the reformer (once the hydrogen production is accomplished) is released anyway at the condenser. Furthermore, the CO purification is easier and the lower temperatures and flowrates at the burner exit makes the reformer operation much more stable with respect to the gases split fraction, eliminating the instability range which prevents the increase of the FC power at intermediate utilization factors. Indeed, the feed water is internally heated and vaporised through the excess water in the reformate. The sensitivity analyses predict that there is a variable distribution of the duties between reformer-condensate and fuel cell, without changing the net heat input.

A high water dilution, on the other hand, is not compatible with a full FC exploitation of the reformate and gives raise to tricky regime-change and instability phenomena at too low cell utilization factor, where the hot gases production and utilization are both enhanced to opposite effects. The details of this behavior are anyway dependent on the absolute ethanol quantity employed, since this value fixes the total power available from the system in any form (electrical or thermal), but we conclude that a ratio of 7 moles of water to 1 mole of alcohol is preferable to a more concentrated 5:1 feed for this power scale. A defined enthalpy optimum is not clearly set, depending on the possibility to recover the condensation heat. The operating optimum depends on the distribution of the thermal loads and on the possibility to distribute the streams appropriately through the split valves. In the present configuration, W/E = 3 is not suitable to cover all the conditions and needs. W/E = 8 is too high. A good compromise is 5 or 7. Nevertheless, for given

operating points (*e.g.* during shower use), it may be advisable to operate at W/E = 3 to drive the thermal power to sanitary water rather than to radiators, but in such a case, the cell load should be decreased since too low hydrogen amount would be available, leaving out of specifications for power load.

The increase of the condenser duty (insensitive to the flue gases split fraction) at the burner gas expenses, makes the total thermal power available at lower temperatures. Our steady-state calculation of a typical radiator-based house heating network shows that there are sufficient operation margins to overcome this limitation even in the worst winter case, bringing the overall system energetic yield to a minimum of 52%, over a theoretical 80%.

The sanitary water production scenario is different and too high condenser duty makes unfeasible reaching the set-point (cases 3 and 6). In all the other cases, however, the hot water demand of 10 L/min are met essentially in two ways: i) decreasing the electrical output to 3 kW for 15 minutes while maintaining the water content at its nominal level or ii) maintaining a high electrical power output and letting the sanitary circuit deplete for as long as 35 minutes. According to different household electrical needs and environmental situations (winter / summer), the switch between this strategy is readily achievable, since the three best cases for the hot water supply (1, 4 and 5) cover both the cases of ethanol dilution with 5 or 7 moles of water at different fuel cell power. Moreover, this calculation is quite conservative since it is supposed that more than half of a family daily consumption is consumed in 30 – 40 minutes. Moreover, when the sanitary water is being produced, the plant efficiency reaches its maximum ideal value, because all the heat dissipated from the reformer goes directly (via the sanitary HX) or indirectly (via the main water reserve) into this circuit.

If the condenser temperature is raised to 55 °C, the cogeneration section gains two advantages: *i)* the steady-state radiators calculation shows an increased thermal recovery (nearly 1 kW of the 21 globally available, and *ii)* the sanitary water circuit can be set to work at no less than 48 °C for at least 35 minutes without sacrificing the electric production. In this context, if a lower hot water

target temperature is maintained, it is also possible to shift the heat balance from the hot gases to the condenser, increasing further (case ‘71’) the overall efficiency to 57%.

Acknowledgements

The authors wish to thank Ing. A. Cogliandro for the helpful suggestions for the section on the energetic assessment of buildings. The authors are indebted with Antonio Pizzonia for support in designing the Aspen Plus flowsheet.

Bibliography

[1] König P, Ivers-Tiffèe E. Increase of the fuel cell system efficiency — Modular testing, analysis and development environment. J Power Sources 2009;190:121–32. doi:10.1016/j.jpowsour.2008.07.045.

[2] Cheng X, Shi Z, Glass N, Zhang L, Zhang J, Song D, et al. A review of PEM hydrogen fuel cell contamination: Impacts, mechanisms, and mitigation. J Power Sources 2007;165:739–56. doi:10.1016/j.jpowsour.2006.12.012.

[3] Kirillov V a., Meshcheryakov VD, Sobyanin V a., Belyaev VD, Amosov YI, Kuzin N a., et al. Bioethanol as a promising fuel for fuel cell power plants. Theor Found Chem Eng 2008;42:1–11. doi:10.1134/S0040579508010016.

[4] Ni M, Leung DYC, Leung MKH. A review on reforming bio-ethanol for hydrogen production. Int J Hydrogen Energy 2007;32:3238–47. doi:10.1016/j.ijhydene.2007.04.038.

[5] Bhat SA, Sadhukhan J. Process Intensification Aspects for Steam Methane Reforming: An Overview. Am Inst Chem Eng 2009;55. doi:10.1002/aic.11687.

[6] Hiblot H, Ziegler D, Fournet R, Glaude PA. Steam reforming of methane in a synthesis gas from biomass gasification. Int J Hydrogen Energy 2016;41:18329–38. doi:10.1016/j.ijhydene.2016.07.226.

[7] Xuan J, Leung MKH, Leung DYC, Ni M. A review of biomass-derived fuel processors for fuel cell systems. Renew Sustain Energy Rev 2009;13:1301–13. doi:10.1016/j.rser.2008.09.027.

[8] Remiro A, Valle B, Oar-arteta L, Aguayo T, Bilbao J, Gayubo AG. Hydrogen production by steam reforming of bio-oil and bio-ethanol mixtures in a continuous thermal-catalytic process. Int J Hydrogen Energy 2014;39:6889–98. doi:10.1016/j.ijhydene.2014.02.137.

[9] Zou J, Yang H, Zeng Z, Wu C, Williams PT, Chen H. Hydrogen production from pyrolysis catalytic reforming of cellulose in the presence of K alkali metal. Int J Hydrogen Energy 2016;41:10598–607. doi:10.1016/j.ijhydene.2016.04.207.

[10] Ma Z, Xiao R, Zhang H. Catalytic steam reforming of bio-oil model compounds for hydrogen-rich gas production using bio-char as catalyst. Int J Hydrogen Energy 2017;42:3579–85. doi:10.1016/j.ijhydene.2016.11.107.

[11] Fuentes-Cortés LF, Avila-Hernàndez A, Serna-Gonzàlez M, Ponce-Ortega JM. Optimal design of CHP systems for housing complexes involving weather and electric market variations. Appl Therm Eng 2015;90:895–906. doi:10.1016/j.applthermaleng.2015.07.074.

[12] Lanzini A, Santarelli M, Orsello G. Residential Solid Oxide Fuel Cell Generator Fuelled by Ethanol: Cell, Stack and System Modelling with a Preliminary Experiment. Fuel Cells 2010:654–75. doi:10.1002/fuce.201000004.

[13] Farra N, Tzanetakis T, Thomson MJ. Experimental Determination of the Efficiency and Emissions of a Residential Microcogeneration System Based on a Stirling Engine and Fueled by Diesel and Ethanol. Energy & Fuels 2012;26:889–900. doi:dx.doi.org/10.1021/ef201468j.

[14] Francesconi J a., Mussati MC, Mato RO, Aguirre P a. Analysis of the energy efficiency of an integrated ethanol processor for PEM fuel cell systems. J Power Sources 2007;167:151–61. doi:10.1016/j.jpowsour.2006.12.109.

[15] Oakley JH, Hoadley a. F a. Industrial scale steam reforming of bioethanol: A conceptual study. Int J Hydrogen Energy 2010;35:8472–85. doi:10.1016/j.ijhydene.2010.05.003.

[16] Rossetti I, Compagnoni M, Torli M. Process simulation and optimization of H 2 production from ethanol steam reforming and its use in fuel cells . 2 . Process analysis and optimization. Chem Eng J 2015;281:1036–44. doi:10.1016/j.cej.2015.08.045.

[17] Rossetti I, Biffi C, Tantardini GF, Raimondi M, Vitto E, Alberti D. 5 kW e + 5 kW t reformer-PEMFC energy generator from bioethanol first data on the fuel processor from a demonstrative project. Int J Hydrogen Energy 2012;37:8499–504. doi:10.1016/j.ijhydene.2012.02.095.

[18] Tripodi A, Pizzonia A, Compagnoni M, Ramis G, Rossetti I. Integrated plant layout for electrical and power cogeneration from diluted biothanol. (Submitted) n.d.

[19] Jablonski A, Lewera A. Improving the efficiency of a direct ethanol fuel cell by a periodic load change. Cuihua Xuebao/Chinese J Catal 2015;36:496–501. doi:10.1016/S1872-2067(14)60226-6.

[20] Murugan S, Horák B. A review of micro combined heat and power systems for residential applications. Renew Sustain Energy Rev 2016;64:144–62. doi:10.1016/j.rser.2016.04.064.

[21] Pehnt M. Environmental impacts of distributed energy systems-The case of micro cogeneration. Environ Sci Policy 2008;11:25–37. doi:10.1016/j.envsci.2007.07.001.

[22] Lauinger D, Caliandro P, Van herle J, Kuhn D. A linear programming approach to the optimization of residential energy systems. J Energy Storage 2016;7:24–37. doi:10.1016/j.est.2016.04.009.
[23] Carboni C, Montanari R. Solar thermal systems: Advantages in domestic integration. Renew Energy 2008;33:1364–73. doi:10.1016/j.renene.2007.07.004.
[24] Liso V, Zhao Y, Yang W, Nielsen MP. Modelling of a solid oxide fuel cell CHP system coupled with a hot water storage tank for a single household. Energies 2015;8:2211–29. doi:10.3390/en8032211.
[25] Vialetto G, Rokni M. Innovative household systems based on solid oxide fuel cells for a northern European climate. Renew Energy 2015;78:146–56. doi:10.1016/j.renene.2015.01.012.
[26] Rosato A, Sibilio S, Ciampi G. Energy, environmental and economic dynamic performance assessment of different micro-cogeneration systems in a residential application. Appl Therm Eng 2013;59:599–617. doi:10.1016/j.applthermaleng.2013.06.022.
[27] Wang Y, Huang Y, Chiremba E, Roskilly AP, Hewitt N, Ding Y, et al. An investigation of a household size trigeneration running with hydrogen. Appl Energy 2011;88:2176–82. doi:10.1016/j.apenergy.2011.01.004.
[28] Esmaili E, Mostafavi E, Mahinpey N. Economic assessment of integrated coal gasification combined cycle with sorbent CO2 capture. Appl Energy 2016;169:341–52. doi:10.1016/j.apenergy.2016.02.035.
[29] Parkinson B, Tabatabaei M, Upham DC, Ballinger B, Greig C, Smart S, et al. Hydrogen production using methane: Techno-economics of decarbonizing fuels and chemicals. Int J Hydrogen Energy 2018;43:2540–55. doi:10.1016/j.ijhydene.2017.12.081.
[30] Mantripragada HC, Rubina ES. Chemical looping for pre-combustion CO2capture - Performance and cost analysis. Energy Procedia 2013;37:618–25. doi:10.1016/j.egypro.2013.05.149.
[31] Blumberg T, Assar M, Morosuk T, Tsatsaronis G. Comparative exergoeconomic evaluation of the latest generation of combined-cycle power plants. Energy Convers Manag 2017;153:616–26. doi:10.1016/j.enconman.2017.10.036.
[32] Schweitzer D, Albrecht FG, Schmid M, Beirow M, Spörl R, Dietrich RU, et al. Process simulation and techno-economic assessment of SER steam gasification for hydrogen production. Int J Hydrogen Energy 2018;43:569–79. doi:10.1016/j.ijhydene.2017.11.001.
[33] Baniasadi E, Toghyani S, Afshari E. Exergetic and exergoeconomic evaluation of a trigeneration system based on natural gas-PEM fuel cell. Int J Hydrogen Energy 2017;42:5327–39. doi:10.1016/j.ijhydene.2016.11.063.
[34] Onovwiona HI, Ugursal VI. Residential cogeneration systems: Review of the current technology. Renew Sustain Energy Rev 2006;10:389–431. doi:10.1016/j.rser.2004.07.005.
[35] ITC-CNR, ENEA according to: UNI TS 11300-1-2/3/4/5 (2016). Http://www.docet.itc.cnr.it/ n.d.
[36] Rossetti I, Lasso J, Compagnoni M, Guido G De. H 2 Production from Bioethanol and its Use in Fuel-Cells. Chem Eng Trans 2015;43:229–34. doi:10.3303/CET1543039.
[37] Tripodi A, Compagnoni M, Ramis G, Rossetti I. Process simulation of hydrogen production by steam reforming of diluted bioethanol solutions: Effect of operating parameters on electrical and thermal cogeneration by using fuel cells. Int J Hydrogen Energy 2017:in press. doi:10.1016/j.ijhydene.2017.04.056.
[38] Ramis G, Rossetti I, Tripodi A, Compagnoni M. Diluted Bioethanol Solutions for the Production of Hydrogen and Ethylene. Chem Eng Trans 2017;57:1663–8. doi:10.3303/CET1757278.
[39] Tripodi A, Compagnoni M, Rossetti I. Kinetic modeling and reactor simulation for ethanol steam reforming. ChemCatChem 2016;8:3804 – 3813. doi:10.1002/cctc.201601075.
[40] Rossini F. Heats of Formation of Simple Organic Molecules. Ind Eng Chem 1937.
[41] Stergaard DS, Svendsen S. Case study of low-temperature heating in an existing single-family house - A test of methods for simulation of heating system temperatures. Energy Build 2016;126:535–44. doi:10.1016/j.enbuild.2016.05.042.
[42] Le Dréau J, Heiselberg P. Energy flexibility of residential buildings using short term heat storage in the thermal mass. Energy 2016;111:991–1002. doi:10.1016/j.energy.2016.05.076.
[43] Thermal Yield Certification (EN-442) of Global VOX-KLASS Radiators. http://www.globalradiatori.it/public/Prodotti/ n.d.
[44] Emission Calculation of Idealclima Radiators (EN-442). Http://www.idealclima.org/ing/emissioni.asp n.d.
[45] Incropera F., DeWitt D. P. Fundamentals of Heat and Mass Transfer. Wiley. New York: 2000.
[46] Application Guide and Catalogue of Watts Thermostatic Mixing Valves. http://wattsindustries.com/Support-Literature-English.aspx n.d.

[47] Liso V, Zhao Y, Brandon N, Nielsen MP, Koer SK. Analysis of the impact of heat-to-power ratio for a SOFC-based mCHP system for residential application under different climate regions in Europe. Int J Hydrogen Energy 2011;36:13715–26. doi:10.1016/j.ijhydene.2011.07.086.
[48] Rhoads WJ, Ji P, Pruden A, Edwards MA. Water heater temperature set point and water use patterns influence Legionella pneumophila and associated microorganisms at the tap. Microbiome 2015;3:67. doi:10.1186/s40168-015-0134-1.
[49] Controller manual of Sime SHP MErP. Www.sime.it/it/it/prodotti/navmultien/ n.d.
[50] Installation instructions of RDZ HPAWS. Www.rdz.it/tipo-Documenti-Riservati/pompe-Di-Calore/ n.d.
[51] Technical Bulletin of Clivet WSAN-XIN. Www.clivet.com n.d.
[52] Rosato A, Sibilio S, Ciampi G. Dynamic performance assessment of a building-integrated cogeneration system for an Italian residential application. Energy Build 2013;64:343–58. doi:10.1016/j.enbuild.2013.05.035.
[53] Rosato A, Sibilio S, Scorpio M. Dynamic performance assessment of a residential building-integrated cogeneration system under different boundary conditions. Part I: Energy analysis. Energy Convers Manag 2014;79:731–48. doi:10.1016/j.enconman.2013.10.001.
[54] Vialetto G, Noro M, Rokni M. Combined micro-cogeneration and electric vehicle system for household application: An energy and economic analysis in a Northern European climate. Int J Hydrogen Energy 2017;42:10285–97. doi:10.1016/j.ijhydene.2017.01.035.
[55] Jahn H-J, Schroer W. Dynamic simulation model of a steam reformer for a residential fuel cell power plant. J Power Sources 2005;150:101–9. doi:10.1016/j.jpowsour.2005.02.012.
[56] Salemme L, Menna L, Simeone M. Thermodynamic analysis of ethanol processors - PEM fuel cell systems. Int J Hydrogen Energy 2010;35:3480–9. doi:10.1016/j.ijhydene.2010.01.119.

Tables and Figures

Reaction	Stoichiometry	Rate Expression
1	$AcH \rightarrow CH_4 + CO$	$r_1 = k_1 e^{-E1/RT} \frac{y_{AcH} y_{H_2}^{0.5} y_{CO}^{-1}}{D^2}$
2	$EtOH + H_2O \rightarrow CH_4 + CO_2 + 2H_2$	$r_2 = k_2 e^{-E2/RT} \frac{y_{AcH} y_{H_2O} y_{CH_4}^{-1}}{D^2}$
3	$CH_4 + 2H_2O \leftrightarrows 4H_2 + CO_2$	$r_3 = k_3 e^{-E3/RT} \frac{y_{H_2O}^2 y_{H_2}^{-2.5} y_{CH_4} - K_{3,eq} y_{H_2}^{1.5} y_{CO_2}}{D^3}$
4	$H_2 + CO_2 \leftrightarrows H_2O + CO$	$r_4 = k_4 e^{-E4/RT} \frac{y_{H_2}^{0.5} y_{CO_2} - K_{4,eq} y_{H_3O} y_{H_2}^{-0.5} y_{CO}}{D^2}$
5	$EtOH \rightarrow AcH + H_2$	$r_5 = k_5 e^{-E5/RT} \frac{y_{EtOH} y_{H_2}^{-0.5}}{D^2}$
6	$EtOH \rightarrow C_2H_4 + H_2O$	$r_6 = k_6 e^{-E6/RT} \frac{y_{EtOH}}{D^3}$
7	$C_2H_4 \rightarrow 2C + H_2$	$r_7 = k_7 e^{-E7/RT} \frac{y_{CH_4} y_{H_2}^{-1.5}}{D^2}$

Table 1: Summary of reforming reactions implemented in the PFR block in the Aspen Plus® simulation. Species concentrations are as molar fractions *y*. D is defined as: $1 + \sum_i K_i \prod_j y^{a_{ij}}$. Equilibrium constants for the reactions 3 and 4 are calculated from the temperature-dependent reactants/products chemical potentials for the given stoichiometry. Other parameters were optimized as described in the given reference [39].

	x					**a**	**b**	**c**
CondS	0.5	0.6	0.7	0.8	0.9			
0	0.42	0.45	0.5	0.7	0.8	2.07	1.89	0.84
140	0.6	0.7	0.75	0.85	1	1.07	0.55	0.62
280	0.85	0.95	0.97	1	-	0	0.47	0.64

Table2: FlueS2 values selected according to *x* and CondS settings. Parameters a, b and c are relative to a parabolic interpolation as: $y = ax^2 + bx + c$.

	x				
CondS	0.5	0.6	0.7	0.8	0.9
0	.25-.40	.25-.42	.25-.45	.25-.50	.25-.50
140	.25-.55	.40-.55	.25-.55	.25-.55	.25-.55
280	.35-.55	.25-.55	.25-.55	.25-.425	-

Table3: FlueS1 ranges allowed for each x and CondS set up.

Radiator element stepwise calculation									
Step	**T_{water} (°C)**	**T_{air}**	**dT**	**T_{water}-20**	**Heat (dT) (W)**	**Heat(T-20)**	**U(dT) (W °C^{-1})**	**U(T-20)**	
0	69.5	31.0	38.5	49.5	114.1	159.8	3.0	3.2	
1	66.8	29.4	37.4	46.8	109.8	148.3	2.9	3.2	
2	64.1	27.8	36.3	44.1	105.5	136.9	2.9	3.1	
3	61.4	26.2	35.2	41.4	101.2	125.8	2.9	3.0	
4	58.7	24.6	34.1	38.7	97.0	114.9	2.8	3.0	
5	56.0	23.0	33.0	36.0	92.8	104.3	2.8	2.9	
6	53.3	21.4	31.9	33.3	88.7	94.0	2.8	2.8	
7	50.6	19.8	30.8	30.6	84.6	83.9	2.7	2.7	
8	47.9	18.2	29.7	27.9	80.6	74.1	2.7	2.7	
9	45.2	16.6	28.6	25.2	76.6	64.7	2.7	2.6	
10	42.5	15.0	27.5	22.5	72.7	55.6	2.6	2.5	
Mean	56	23	33	36	93.1	105.7	2.8	2.9	
Water flow (l/h)					3.0	3.6			
Air flow (m^3/h)					17.4	19.8			
Theoretical Calculation (based on air at 20 °C)									
L (m)	**S (m^2)**	**β (K^{-1})**	***μ/ρ* (Pa s m^3 kg^{-1})**	**Gr**	**k (W m^{-1} °C^{-1})**	**cp (J kg^{-1} °C^{-1})**	**Pr**	**Nu**	**h (W m^{-2} °C^{-1})**
0.8	0.65	0.0033	1.6×10^{-5}	$2.13\times10^{+9}$	0.026	1200	0.86	148	4.8

Table 4: Relevant parameters for a single radiator element calculation, essential to input a plausible value of *u* to compile in the AP forms. Values are relative to case '1' of Tables above, with a reference radiator power of 162 W for <dT>=50 °C.

Model house heat dispersion according to the DOCET algorithm					
House general data					
Location	Milan, Italy				
Climate Code	E 2404				
Type	Detached house				
Building period	1986 – 1991				
External color	Medium gradation				
Non-heated spaces					
Under floor	Cellar, car box				
Ceiling	Roof				
House level	Staircase				
Geometric Data					
Building Storey	**number**	**Height (m)**			
Storey height (m)	2	3			
Surface (m^2)	100				
Plant dimensions		**N**	**E**	**S**	**W**
Equivalent length (m)		10	10	10	10
Walls	**U (W/m^2K)**	**A (m^2)**			
		N	**E**	**S**	**W**
External walls	1.14	56	53	54	54
Windows – French door	2.9	3.9	6.9	5.9	5.9
		total			
Staircase walls	1.11	24			
Floor	1.25	120			
Ceiling	1.50	120			
Total	**Volume (m^3)**	**A (m^2)**			
Gross dimensions	823	554			
Overall Results	**total**	**Dec-Feb**	**Mar-May**	**Jun-Aug**	**Sept-Nov**
Conductive dispersion (W/K)	587				
Convective dispersion (W/K)	30				
House time constant (h)	41.9				
Heating power required(kWh)	30160	18710	4760	0	6690
Classification	**439 kWh/m^2 per year (F)**				

Table 5: Summary of the key parameters and results of the calculation of a model house in the Northern Italy climate. Data relative to summer cooling requirements have been omitted, but they are nevertheless included in the classification result according to the methodology adopted by law. Thermal transmittance of window panes and walls is not shown for simplicity, since its value is automatically taken into account by the algorithm to calculate the global dispersion. Other calculation assumptions can be found and verified in the cited document and references therein.

Block	Balances	Bounds
Reservoir water (R)	$\frac{\partial T_R}{\partial t} = \left(R5 \times T_{R5} + R7 \times T_{R7} - R1 \times T_R - \frac{Q_{R-S}}{c_p} - \frac{Q_{R-ext}}{c_p} \right) \frac{1}{M_R}$	$M_R \equiv M_{R0}$ $R7 = R5 \times (1 - D)$
Condenser HX (C)	$\frac{\partial T_{R,C}}{\partial t} = \left(R0 \times T_R - R2 \times T_{R2} + \frac{Q_{Cond}}{c_p} \right) \frac{1}{M_{R,C}}$ $\frac{\partial T_C}{\partial t} = \left(C \times T_{C,in} - C \times T_{C,out} - \frac{Q_{Cond}}{c_p} \right) \frac{1}{M_C}$ $T_{R2} = T_{R,C} + {Q'}/_{R2}; T_{C,out} = T_C - {Q''}/_{C}$	$R2 = R0$ $Q_{Cond} = Q' + Q''$
Fuel Cell HX (FC)	$\frac{\partial T_{R,FC}}{\partial t} = \left(R2 \times T_{R2} - R3 \times T_{R3} + \frac{Q_{FC}}{c_p} \right) \frac{1}{M_{R,FC}}$ $\frac{\partial T_{FC}}{\partial t} = \left(FC \times T_{FC,in} - FC \times T_{FC,out} - \frac{Q_{FC}}{c_p} \right) \frac{1}{M_{FC}}$ $T_{R3} = T_{R,FC} + {Q'}/_{R2}; T_{FC,out} = T_{FC} - {Q''}/_{FC}$	$R3 = R2$ $Q_{FC} = Q' + Q''$
Flue Gas HX (G)	$\frac{\partial T_{R,G}}{\partial t} = \left(R3 \times T_{R3} - R3 \times T_{R5} + \frac{Q_{Gas}}{c_p} \right) \frac{1}{M_{R,G}}$ $\frac{\partial T_G}{\partial t} = \left(G \times T_{G,in} - G \times T_{G,out} - \frac{Q_{Gas}}{c_{p,gas}} \right) \frac{1}{M_G}$ $T_{R5} = T_{R,G} + {Q'}/_{R3}; T_{G,out} = T_G - {Q''}/_{FG}$	$R5 = R3$ $Q_{Gas} = Q' + Q''$
Sanitary HX (X)	$\frac{\partial T_{R,X}}{\partial t} = \left(R6 \times T_{R3} - R6 \times T_{R5} - \frac{Q_X}{c_p} \right) \frac{1}{M_{R,X}}$ $\frac{\partial T_{S,X}}{\partial t} = \left(S1 \times T_S - S2 \times T_{S2} + \frac{Q_X}{c_p} \right) \frac{1}{M_{S,X}}$ $T_{R5} = T_{R,X} - {Q'}/_{R6}; T_{S,2} = T_{S,X} + {Q''}/_{S1}$	$R6 = R5 \times D$ $S2 = S1$ $S2 = S3 \times M$ $Q_X = Q' + Q''$
Sanitary Water (S)	$\frac{\partial T_S}{\partial t} = \left(S4 \times T_{S4} - S4 \times T_S + \frac{Q_{R-S}}{c_p} \right) \frac{1}{M_S}$ $\frac{\partial M_S}{\partial t} = S4 - S1$	$dep = M \times 0.95$ $S4 = S3 \times (M - dep)$ $S2 = S1$ $M_s \geq M_{s0} \times 0.5$
D valve	$\frac{\partial D}{\partial t} = -\rho(T_{S2} - T_{setpt})$	$0.1 < D < 0.95$

Table 6: Mathematical model for the cogeneration – sanitary system dynamic simulation. Refer to Figures 3-4 for the block and stream names. Water flowrates are indicated with the stream name (e.g. R1, S2). Enthalpy content of a stream is conveniently assumed to be 0 at 0 °C. Flowrates C and FC relative to condenser and fuel cell hot side are fictitious, and coupled to very large specific heat values to take into account the latent heat transfer, while the water volumes are fixed equal to the cold side one. Gas mass in the 'G' HX is one tenth of the water mass, and the 'FG' flow is retrieved by the AP simulation for every case. The mixing factor M is fixed at 0.9. Apex for duties refer to the fact that HXs are calculated as split into two sides.

Block	Water volume (L)	Circulating water flow (L/min)	Working Temperatures (°C)	Heat exchange coefficient *UA* (W/°C)
Main water reservoir	800	8 – 20	40 – 45	Sanitary Side / Environment 200 / 10
Sanitary Reserve	300	10.2	5 – 45	Reservoir / Sanitary Heater 200 / 500
Condenser HX cold side	5	8 – 20	40 – 50	600 (*)
FC HX cold side	1	8 – 20	45 – 70	250 (*)
Flues HX cold side	5	8 – 20	50 – 80	20 (*)
Sanitary water heater	5	Hot side / Cold Side 8 – 20 / 10	20 – 60	500
Radiator Element	na	2 – 4	80 – 30	3

Table7: Summary of nominal specifications for the cogeneration system. (*) *UA* data are first-guess values and are adjusted within the calculation to meet the specified heat duties.

Block	Temperature (°C)		Pressure (bar)	Duty (kW)	Hydrogen Flow (mol/h)	
	In	Out			In	Out
Reformer	567	500 – 670	2.0	3 – 3.7	0	185 – 245
FPHX	105	111	2.0		0	0
AUTOHX	111	na	2.0 – 1.8	5.1 – 10	0	0
HTWGS	350	371	2.0	na	na	na
LTWGS	280	281	2.0	na	na	na
Methanator	210	216	2.0	na	na	202 – 261
Condenser	216	50 – 55	1.8	3.7 – 7.8	202 – 261	202 – 261
PEMFC	80	80	1.8	7.8 – 12.6	202 – 261	na
Burner	80	1050 – 1400	1.8	0	na	0
FLUEHX	240 – 860	80	1.8 – 1.0	1.3 – 10.4	0	0

Table 8: Summary of key specifications and results for the SR system fed with 420 mol/h of Ethanol. Ranges of varying parameter refer to the working cases discussed.

Case	Flues frac to SR	FC *x*	E:W dilution (mol/mol)	Condenser heat (kW)	Condenser Temp (°C)	FC power (kW_{el})	FC heat (kW_{th})	FC Temp (°C)	Flues heat (kW_{th})	Flues Temp (°C)
1	0.425	0.8	1:5	3.9	50	4.9	7.4	80	5.6	544
4	0.3	0.5	1:5	3.8	50	3.1	4.7	80	10.4	863
2	0.475	0.8	1:7	5.8	50	5.0	7.5	80	2.7	296
5	0.35	0.5	1:7	5.7	50	3.3	4.9	80	8.1	699
3	0.525	0.7	1:9	7.6	50	4.9	7.3	80	1.3	179
6	0.275	0.6	1:9	7.8	50	3.5	5.3	80	3.8	359
7	0.4	0.9	1:5	4.1	50	5.0	7.6	80	4.4	455
8	0.4	0.9	1:7	6.1	50	5.0	7.5	80	1.9	242
11	0.425	0.8	1:5	3.8	55	4.9	7.4	80	5.6	537
41	0.3	0.5	1:5	3.7	55	3.1	4.7	80	10.4	860
21	0.475	0.8	1:7	5.7	55	5.0	7.5	80	2.8	297
51	0.35	0.5	1:7	5.5	55	3.3	4.9	80	8.1	695
31	0.525	0.7	1:9	7.4	55	4.9	7.3	80	1.4	183
61	0.275	0.6	1:9	7.7	55	3.5	5.3	80	3.8	360
71	0.4	0.9	1:5	4.0	55	5.0	7.6	80	4.4	451
81	0.4	0.9	1:7	5.9	55	5.0	7.5	80	1.9	240

Table9: Reference working points for the steady state of the cogeneration system.

Case	Radiator single element					Total		Dissipator		Condenser		Water Circuit		
	Water T_{in} (°C)	Water T_{out} (°C)	Air T_{out} (°C)	Heat calc(*) (W)	ref(**) (W)	Heat rad (kW)	diss (W)	Air T_{out} (°C)	Fan Work (W)	Hot T_{out} (°C)	Cold T_{out} (°C)	Flow total (°C)	RS1 split (L/L)	Reserve elem. n°
1	69.5	42.5	31.4	101	104	9.5	7.5	26.5	26.5	50	45.5	11.9	0.35	50
4	70.5	43.0	31.7	103	107	9.6	9.3	31.7	31.7	50	45.3	11.9	0.27	67
2	69.1	42.3	31.3	101	103	9.4	6.6	24.2	24.2	50	45.8	16.7	0.62	23
5	70.4	42.9	31.7	103	107	9.6	9.1	31.2	31.2	50	45.9	16.0	0.52	47
3	69.9	42.7	31.5	102	105	9.5	6.7	24.5	24.5	50	45.9	21.7	0.76	2
6	70.7	43.1	31.8	104	108	9.6	7.3	26.0	26.0	50	46.1	21.7	0.76	5
11	70.6	43.0	31.7	103	107	9.6	6.5	23.8	23.8	50	45.7	11.9	0.42	34
41	70.0	42.7	31.5	102	106	9.4	6.0	22.4	22.4	50	46.0	17.0	0.67	11
21	74.5	44.9	32.9	111	118	10.3	6.5	23.8	23.8	55	49.7	13.8	0.45	46
51	73.8	44.5	32.7	109	116	10.1	8.6	29.8	29.8	55	49.6	13.8	0.35	72
31	73.9	44.6	32.7	110	117	10.1	5.8	21.9	21.9	55	50.4	17.7	0.64	23
61	74.0	44.6	32.7	110	117	10.3	8.3	28.9	28.9	55	50.3	17.7	0.55	52
71	74.6	44.9	32.9	111	119	10.3	5.8	21.9	21.9	55	50.8	21.7	0.76	4
81	74.8	45.0	33.0	111	119	10.3	6.5	23.8	23.8	55	51.0	21.7	0.75	8

Table10: Performance of the cogeneration system in relation to the power outputs of Table 1. Water flowrate in each radiator element is fixed at 3.3 L/h, and the total elements are 91 (the air flow is set to 18 m^3/h for each element, and its lowest temperature is assumed to be 15 °C). External cooling air for these winter cases is 5 °C. (*) Calculated according to table 4 – (**) Calculated at fixed water temperature (inlet) and fixed air temperature (20 °C).

Case	Water		Air			Heat Exchanger		Fan
	T_{in} (°C)	T_{out} (°C)	T_{in} (°C)	T_{out} (°C)	Flow (kg/h)	Heat (kW)	Area (m^2)	Power (W)
11 (summer)	62	46	25	48	2600	16.5	95	455
4 (summer)	63	41	25	51	2600	18.6	132	460
4 (winter)	52	41	5	31	1260	9.3	33	211

Table 11: Design cases for the residual power dissipater. Heat exchange coefficient U is fixed at 10 W/(m^2°C) and the fan power is calculated for an air-side pressure drop of 5 mbar. Air is assumed as dry.

Case	Electrical η (%)	Thermal η (%)	Total η (%)	Maximalη (%)
1	18.5	35.5	53.9	81.9
4	11.7	35.9	47.6	82.4
2	18.8	35.4	54.2	79.1
5	12.3	35.9	48.2	82.4
3	18.3	35.6	53.9	79.1
6	13.3	36.1	49.4	76.7
7	18.9	36.1	55.0	79.3
8	18.7	35.4	54.1	76.6
11	18.4	38.5	56.9	81.3
41	11.7	38.0	49.7	82.0
21	18.8	38.1	56.8	78.6
51	12.3	38.5	50.8	81.9
31	18.3	38.6	56.9	78.7
61	13.3	38.6	51.9	76.2
71	18.9	37.9	56.8	78.7
81	18.7	38.4	57.1	76.0

Table 12: Efficiency (η) of the tested working cases. Enthalpy content of ethanol was set to 1370 kJ/mol.

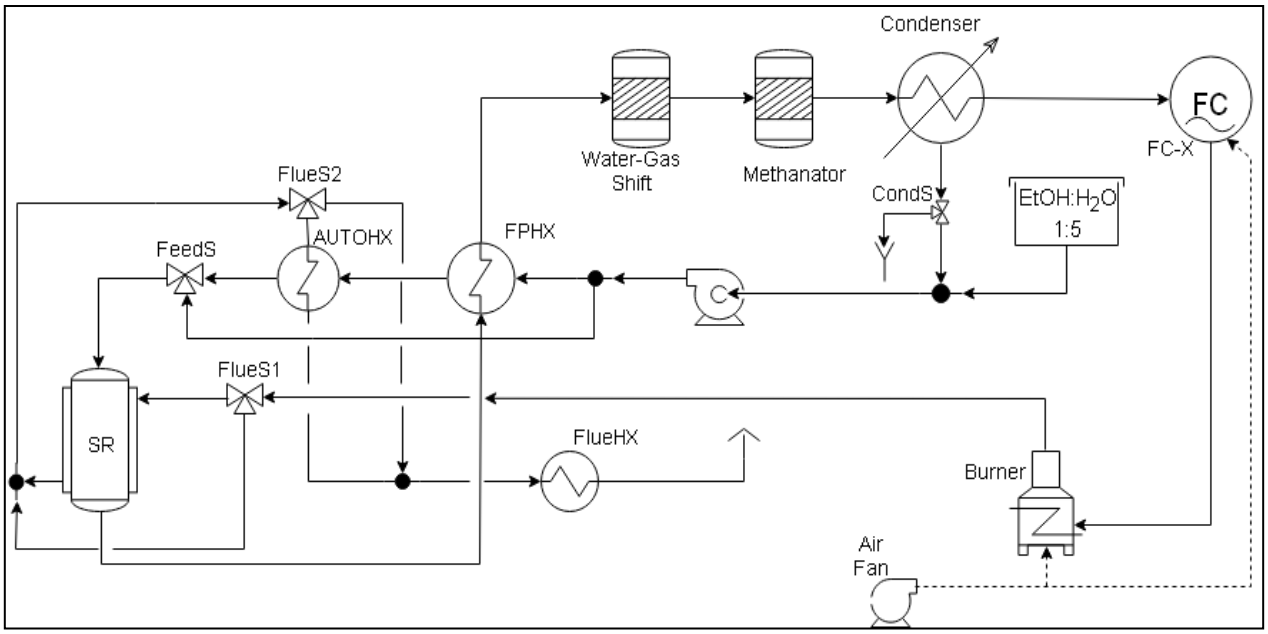

Figure 1: Simplified PFD of the ethanol reforming system.

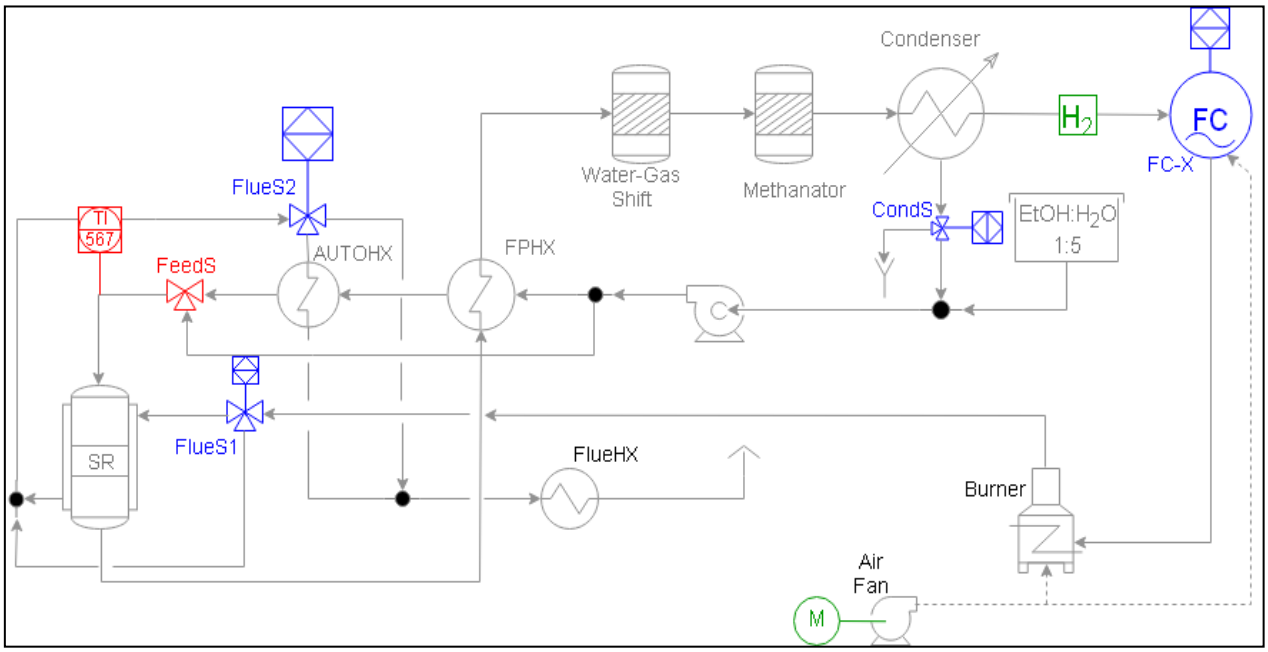

Figure 2: PFD with highlighted controls. The same color indicates the connected variables (red: design spec. green and blue: calculators).

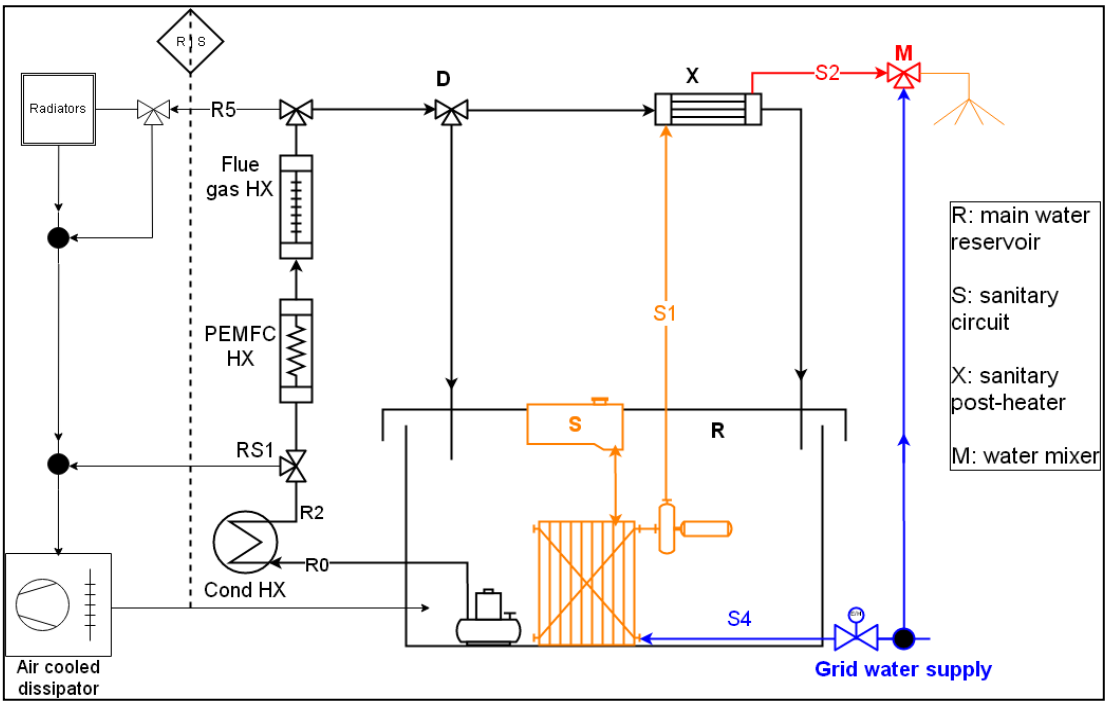

Figure 3: PFD of the cogeneration system (radiators section left of the R|S flag). The representative tap M is set to mix 9 L/min of hot water with 1 L/min of cold water in all the discussed cases. Sanitary circuit volume is supposed to be in perfect thermal contact with the reservoir.

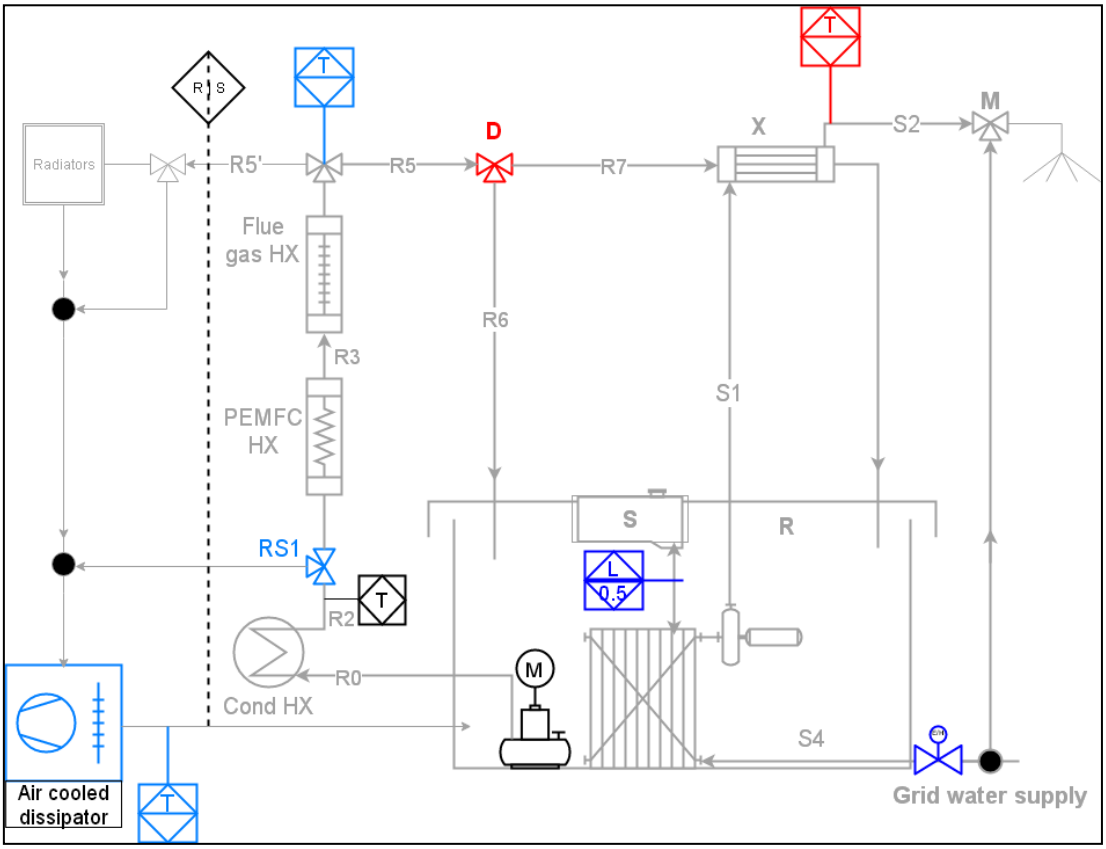

Figure 4: PFD with highlighted controls. Connected variables are of like color (light blue: design spec., red and blue: customized). Notice that, when sanitary water is needed, the dissipater is switched off, the RS1 control is not active and there is no flow from the reservoir to the radiators section (*i.e.* R5'=0 and R5=R0).

a)

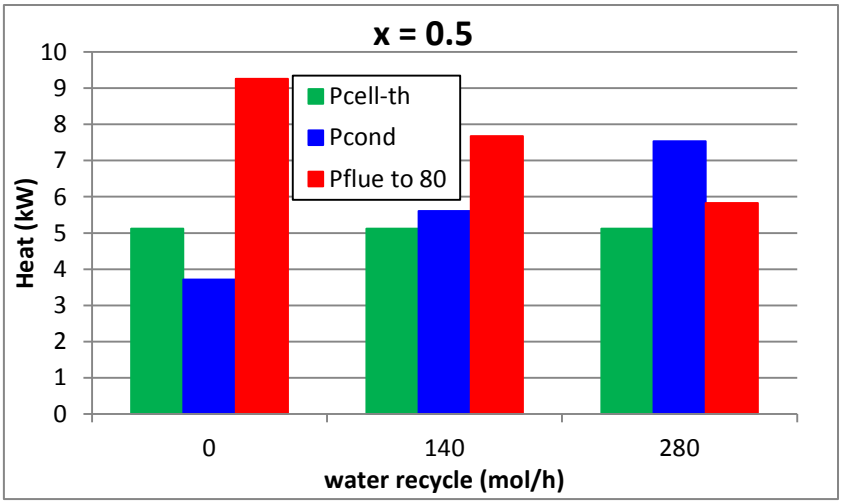

b)

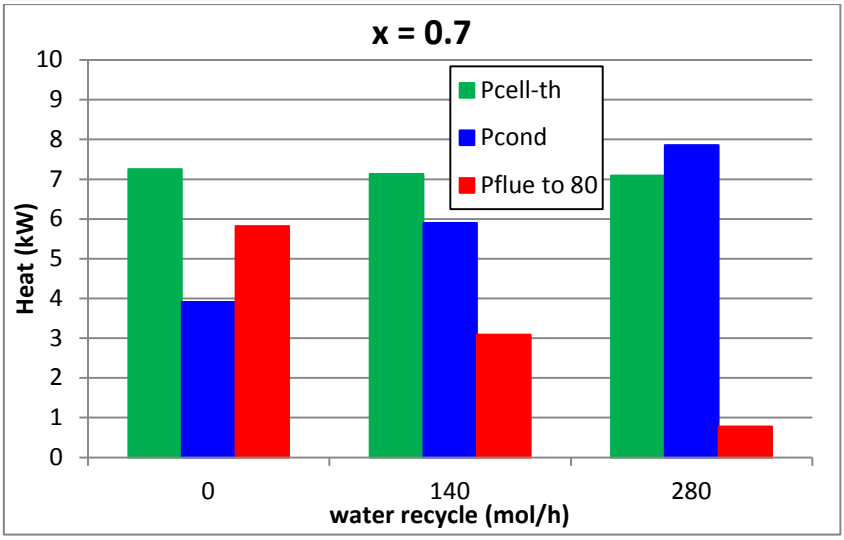

c)

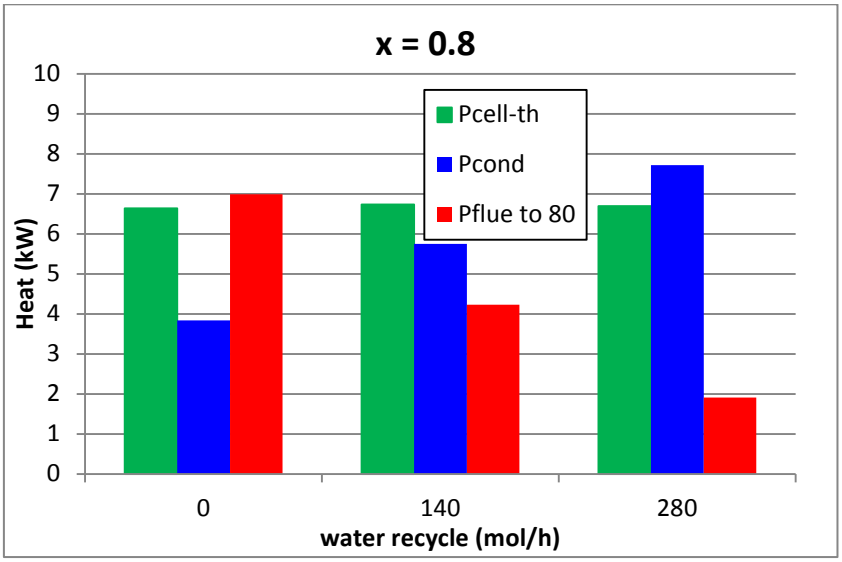

Figure 5: Distribution of the system power outputs, fixing the flue gas flow into the reformer to the 40% of the total burner exit.

a)

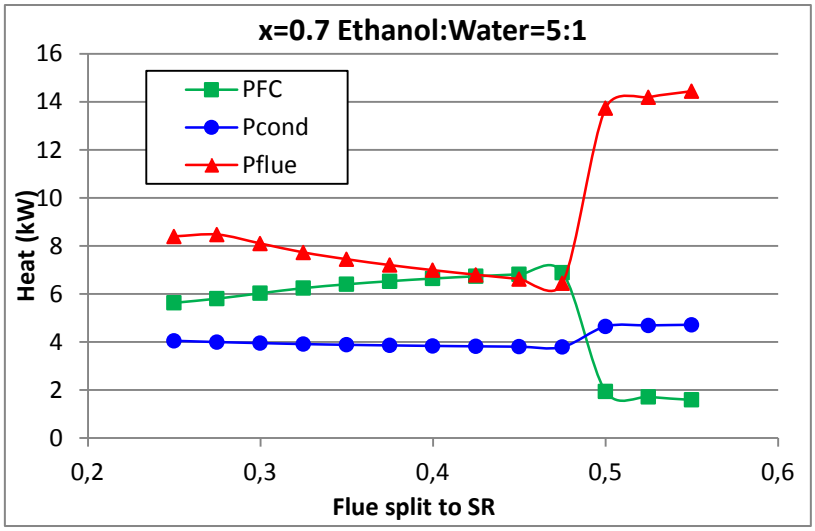

b)

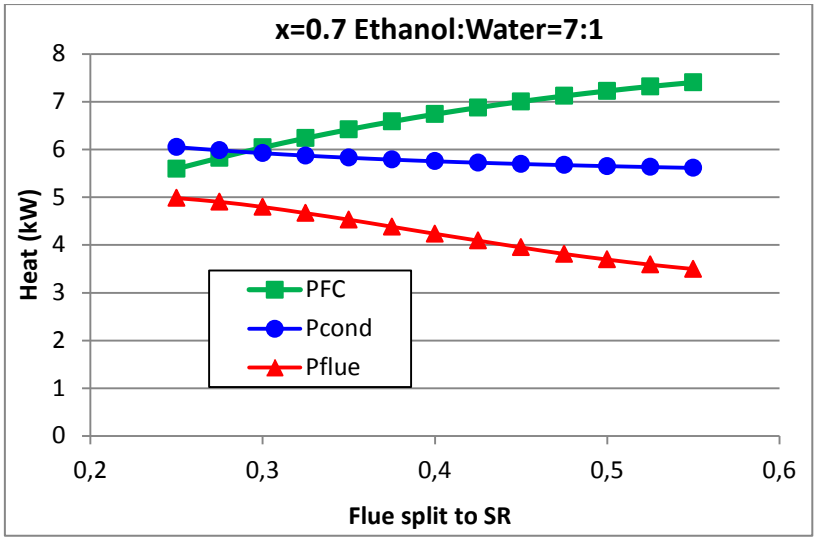

c)

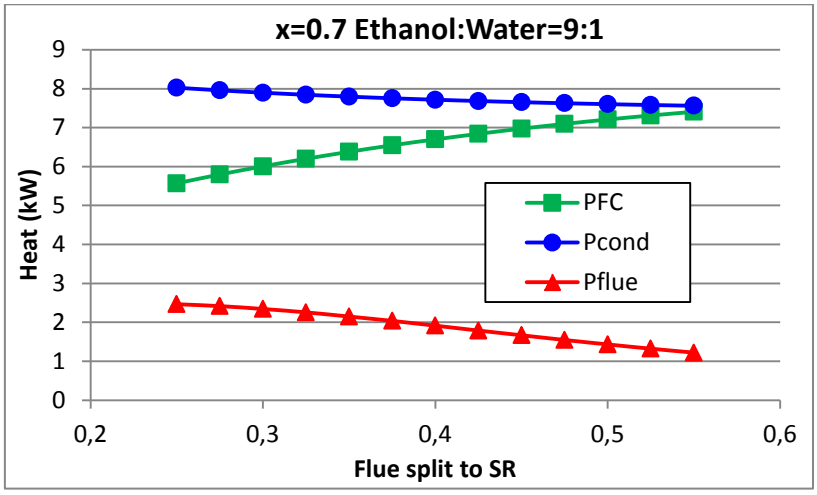

Figure 6: Power output distribution at fixed *x*= 0.7 and variable ethanol dilution for all the tested flue gas splits in the reformer jacket: the redistribution is between the cell power and the residual exhausts enthalpy. Abnormal system behavior at low *x* and high reformer heat input is due a regime change in the reforming chemistry itself, with loss of the hydrogen production.

a)

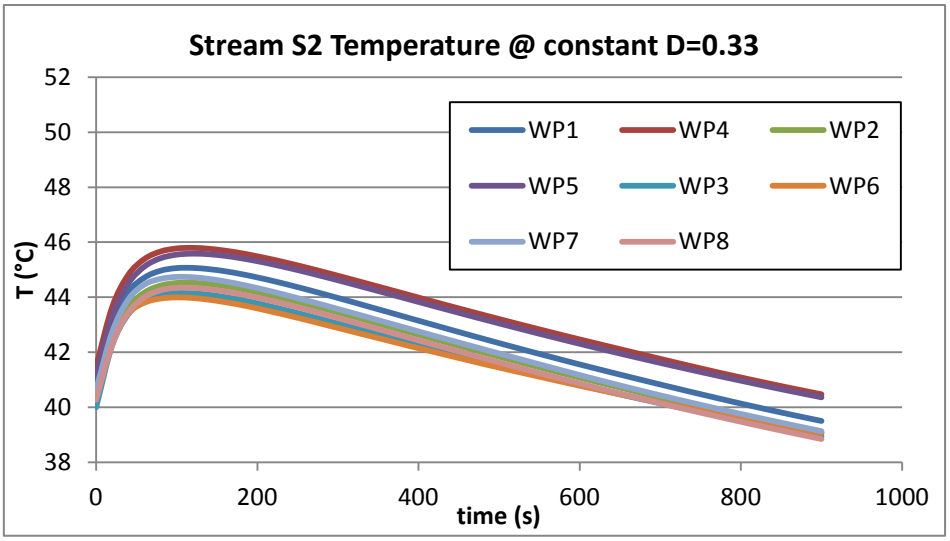

b)

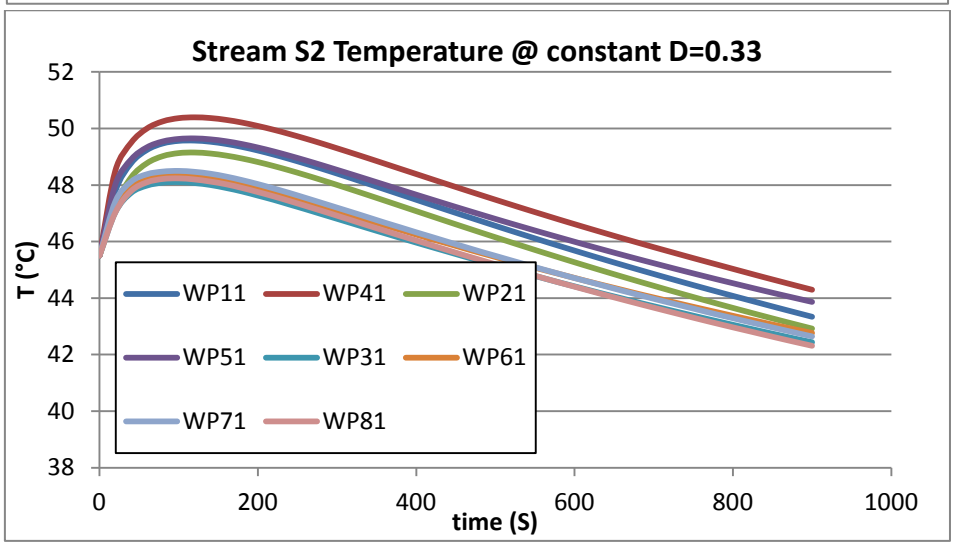

Figure 7: Sanitary water temperature achieved for the cases of Tables 8 and 9 over time, fixing the hot circulating water split ('D' in Figure 3) between the reservoir and the sanitary HX to 0.33. Different starting conditions are determined by the reservoir set point (40 °C top, 45 °C bottom).

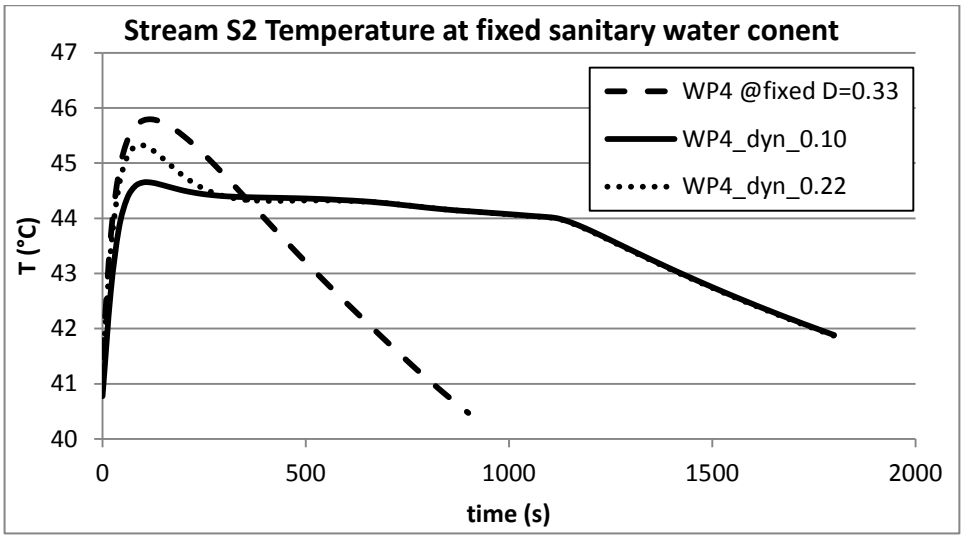

Figure 8: Sanitary water temperature achieved fixing the initial 'D' partition and letting then this parameter vary at constant proportional gain for a chosen case.

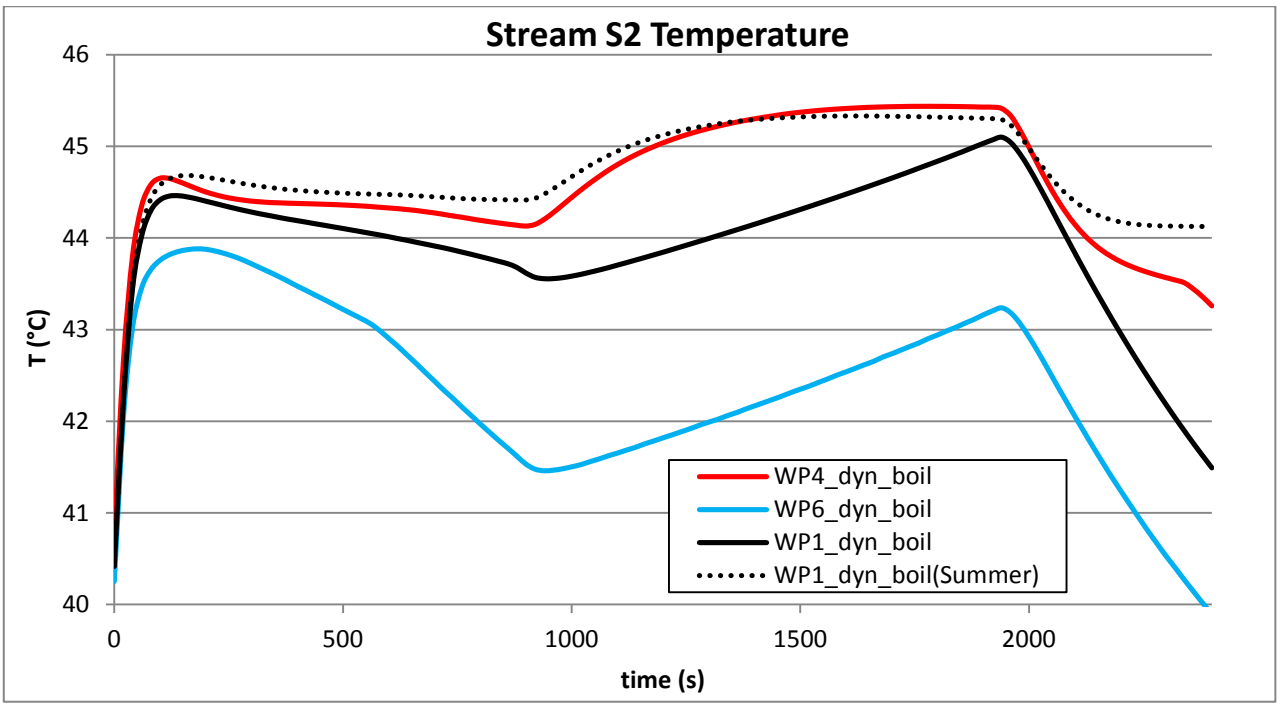

Figure 9: Hot water delivery as the cold water supply is discontinued after 15 minutes and restarted only when the sanitary circuit volume (not shown) falls at half its initial value. 'Summer' case corresponds to a network water supply at 15 °C and an external air temperature at 25 °C.

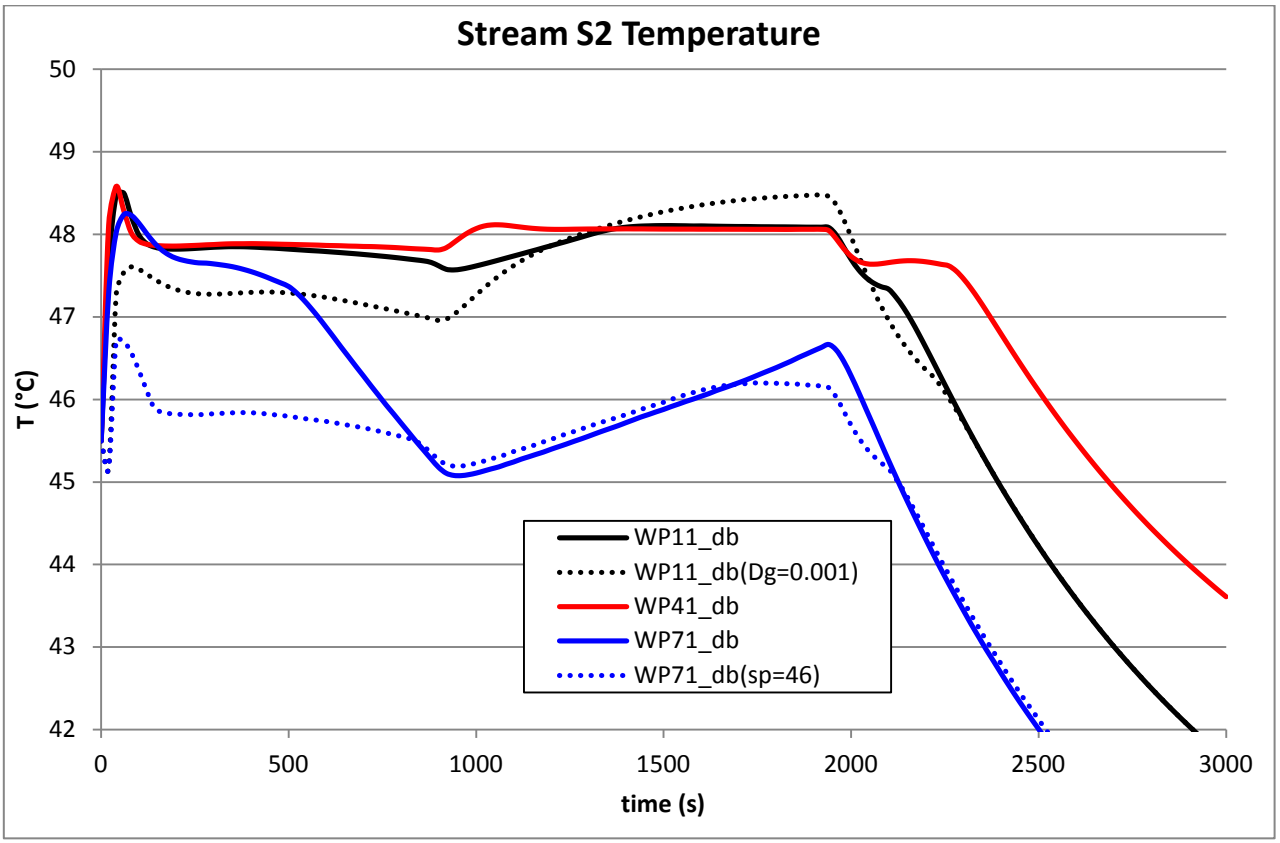

Figure 10: Hot water delivery over time, when the reservoir and the sanitary circuit water is kept initially at 45 °C instead of 40 °C. Working mode '11' is also tested with different gains of the 'D' valve, and the '71' case with a lower setpoint.

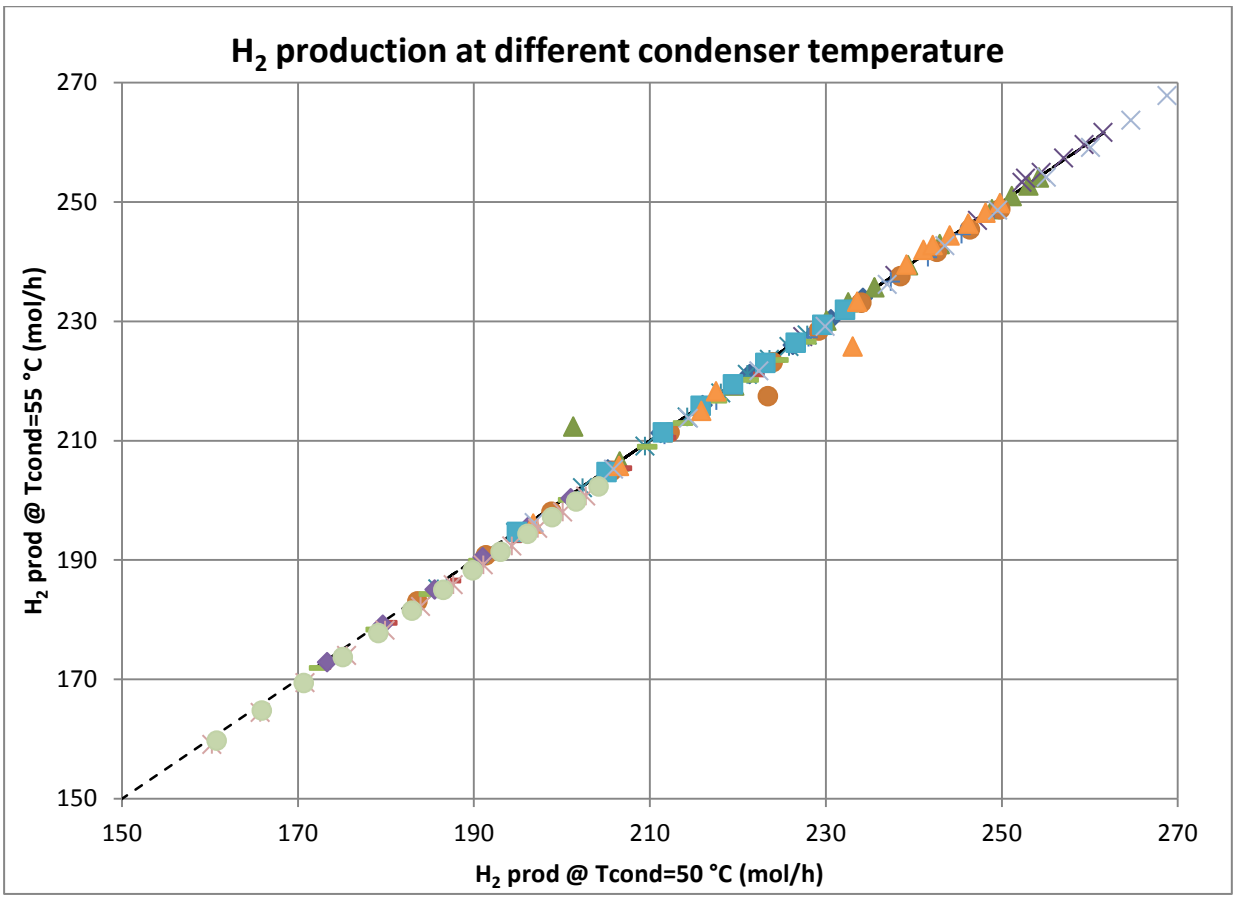

Figure 11: Global comparison of the hydrogen molar flow exiting the steam reformer when the reformate condenser is at 50 °C (x axis values) or at 55 °C (y axis values).

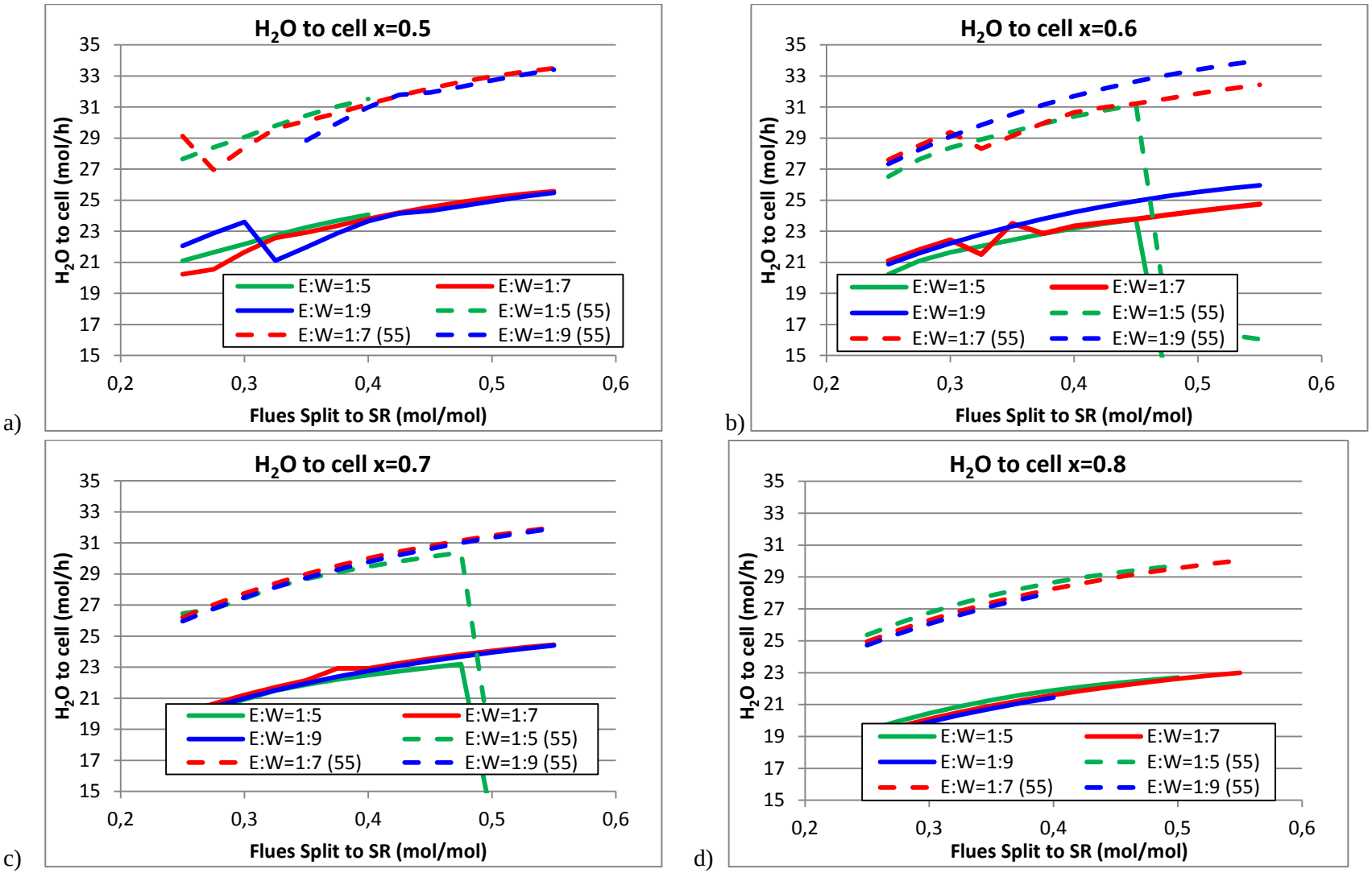

Figures 12: Absolute quantities of water left in the condenser vapor phase as a function of the hot gases routed to the reformer for different cell utilization factors (*x*). Dashed lines indicate the simulations run with the condenser at 55 °C instead of 50 °C. Over-range spikes are due to a too high hot gas flow for the considered feed dilution.

a)

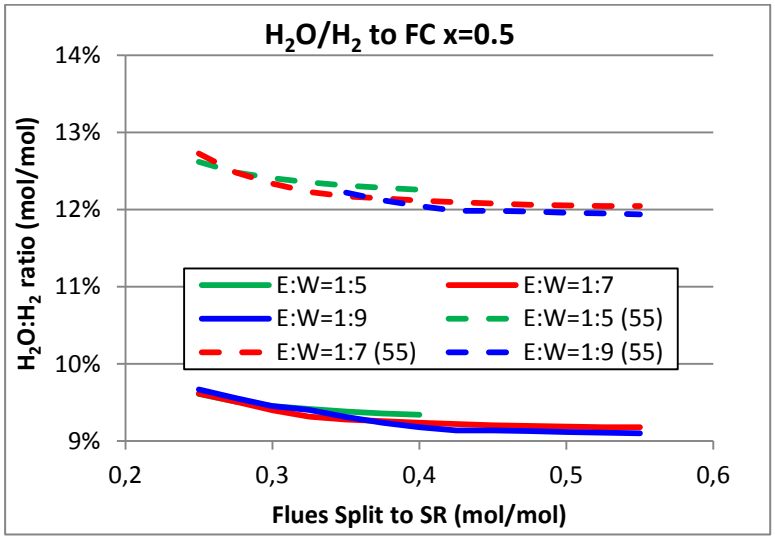
H2O/H2 to FC x=0.5
H2O:H2 ratio (mol/mol)
14%
13%
12%
11%
10%
9%
0,2
0,3
0,4
0,5
0,6
Flues Split to SR (mol/mol)
E:W=1:5
E:W=1:7
E:W=1:9
E:W=1:5 (55)
E:W=1:7 (55)
E:W=1:9 (55)

b)

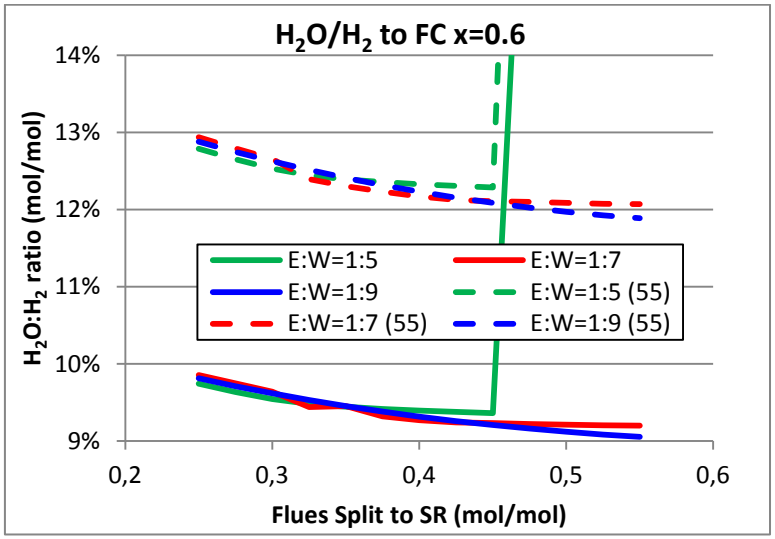
H2O/H2 to FC x=0.6
H2O:H2 ratio (mol/mol)
14%
13%
12%
11%
10%
9%
0,2
0,3
0,4
0,5
0,6
Flues Split to SR (mol/mol)
E:W=1:5
E:W=1:7
E:W=1:9
E:W=1:5 (55)
E:W=1:7 (55)
E:W=1:9 (55)

c)

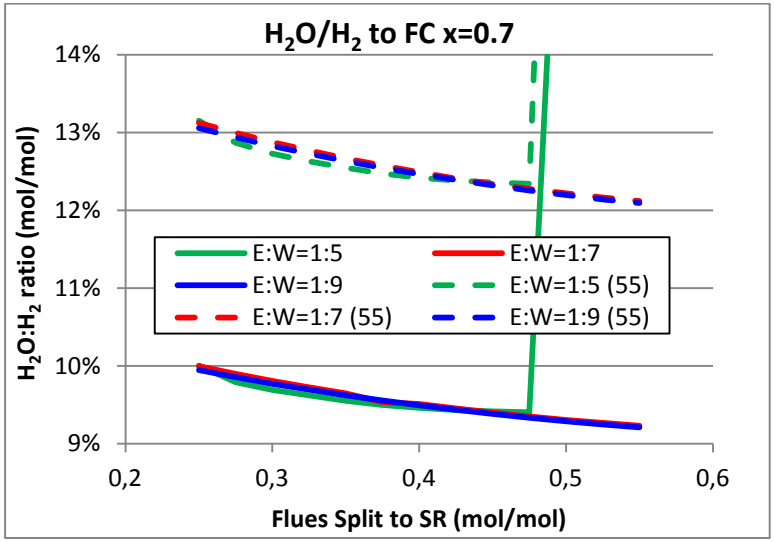
H2O/H2 to FC x=0.7
H2O:H2 ratio (mol/mol)
14%
13%
12%
11%
10%
9%
0,2
0,3
0,4
0,5
0,6
Flues Split to SR (mol/mol)
E:W=1:5
E:W=1:7
E:W=1:9
E:W=1:5 (55)
E:W=1:7 (55)
E:W=1:9 (55)

d)

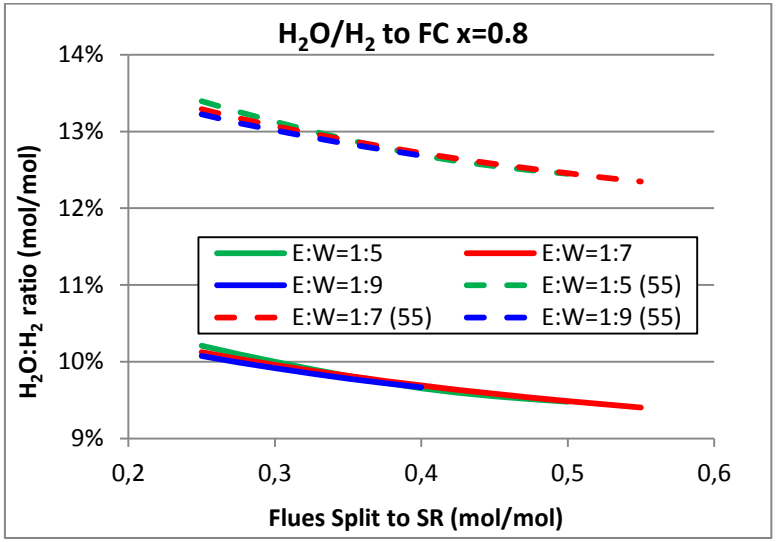
H2O/H2 to FC x=0.8
H2O:H2 ratio (mol/mol)
14%
13%
12%
11%
10%
9%
0,2
0,3
0,4
0,5
0,6
Flues Split to SR (mol/mol)
E:W=1:5
E:W=1:7
E:W=1:9
E:W=1:5 (55)
E:W=1:7 (55)
E:W=1:9 (55)

Figure 13: Ratio of the water vapor to the hydrogen at the FC inlet as hotter reforming condition yield less hydrogen and a mixture with higher dew point. Dashed lines indicate the simulations run with the condenser at 55 °C instead of 50 °C.